מכון ויצמן למדע
WEIZMANN INSTITUTE OF SCIENCE

Molecular characterization of human cytomegalovirus infection with single-cell transcriptomics

Document Version:
Accepted author manuscript (peer-reviewed)

Citation for published version:
Schwartz, M, Shnayder, M, Nachshon, A, Arazi, T, Kitsberg, Y, Levi Samia, R, Lavi, M, Kuint, R, Tsabari, R & Stern-Ginossar, N 2023, 'Molecular characterization of human cytomegalovirus infection with single-cell transcriptomics', *Nature Microbiology*, vol. 8, pp. 455-468. https://doi.org/10.1038/s41564-023-01325-x

Total number of authors:
10

Digital Object Identifier (DOI):
10.1038/s41564-023-01325-x

Published In:
Nature Microbiology

License:
Unspecified

General rights
@ 2020 This manuscript version is made available under the above license via The Weizmann Institute of Science Open Access Collection is retained by the author(s) and / or other copyright owners and it is a condition of accessing these publications that users recognize and abide by the legal requirements associated with these rights.

How does open access to this work benefit you?
Let us know @ library@weizmann.ac.il

Take down policy
The Weizmann Institute of Science has made every reasonable effort to ensure that Weizmann Institute of Science content complies with copyright restrictions. If you believe that the public display of this file breaches copyright please contact library@weizmann.ac.il providing details, and we will remove access to the work immediately and investigate your claim.

(article begins on next page)

1

Figure or Table # Please group Extended Data items by type, in sequential order. Total number of items (Figs. + Tables) must not exceed 10.	Figure/Table title One sentence only	Filename Whole original file name including extension. i.e.: Smith_ED_Fig1.jpg	Figure/Table Legend If you are citing a reference for the first time in these legends, please include all new references in the main text Methods References section, and carry on the numbering from the main References section of the paper. If your paper does not have a Methods section, include all new references at the end of the main Reference list.
Extended Data Fig. 1	Productive and non-productive infection in monocyte derived macrophages.	Schwartz_ED_Fig1.jpg	**a**. Gating strategy used to determine the single-cell population for all flow cytometry analyses of GFP-HCMV infected monocytes and PMA-induced MDMs. **b**. Flow cytometry analysis of primary CD14+ monocytes treated with the indicated treatments and infected with HCMV-GFP. Analysis was performed at 3dpi. Blue and red gates mark the GFP-dim and GFP-bright populations, respectively, and their percentage is noted. **c**. Gating strategy used to determine the single-cell population for flow cytometry analyses of GFP-HCMV infected M-CSF and GM-CSF/IL-4 treated monocytes. **d**. Flow cytometry analysis of CD11b surface expression in PMA and M-CSF treated monocytes and of CD11c surface expression in GM-CSF/IL-4 treated monocytes compared to primary CD14+ monocytes. Shown is a representative of two biological replicates with similar results. **e**. Flow cytometry analysis of PMA-induced monocyte-derived macrophages

			(MDMs) at different times following infection with HCMV-GFP. **f**. Measurements of infectious virus in supernatants from PMA-induced MDMs and from monocytes infected with HCMV-GFP at different times post infection. NA, not assayed. **g**. Microscopy image of PMA-induced MDMs at 3 dpi with HCMV-GFP. Scale bar is 100µm. Shown is a representative of two biological replicates. **h.** Flow cytometry analysis of PMA-induced MDMs infected with HCMV-GFP at 3 dpi showing the size, measured by forward scatter (FSC), of mock-infected, GFP-dim and GFP-bright cells. **i**. Flow cytometry plot showing the gates used to sort GFP-bright (red gate) and GFP-dim (blue gate) HCMV-GFP infected PMA-induced MDMs at 4 dpi. **j**. digital droplet PCR (ddPCR) results of GFP-dim and GFP-bright HCMV-GFP infected PMA-MDMs at 4 dpi. Upper panel shows detection of viral DNA, lower panel reflects detection of cellular genomes. The magenta line marks the threshold. **k-l**. Measurements of viral genomes by ddPCR from GFP-dim and GFP-bright FACS-sorted populations of monocytes treated with M-CSF (**i**) or GM-CSF/IL-4 (**j**). ddPCR graph is a representative of two biological replicates and shows the mean and 95% CV of poisson distribution of >10,000 PCR

			droplets. **m.** Microscopy image of HCMV-GFP infected BAL cells at 2dpi. Scale bar is 10µm. Shown is a representative of four biological replicates. **n.** Flow cytometry analysis of CD14 surface expression in BAL cells enriched for macrophages. Stained and unstained cells are in green and gray, respectively. **o.** Gating strategy used to determine the single-cell population for flow cytometry analyses of GFP-HCMV infected BAL macrophages.
Extended Data Fig. 2	Single cell transcriptome analyses of HCMV infected monocytes and MDMS	Schwartz_ED_Fig2.eps	**a.** Projection of mock-infected and HCMV-GFP infected CD14+ monocytes (n=68 and n=803, respectively) and MDMs (n=540 and n=1815, respectively) from the indicated time points, based on cellular and viral gene expression, colors indicate cell types and time post infection HCMV-infected cells are plotted in gray. **b.** Heatmap depicting the 40 most significantly increased genes between 5hpi infected and mock-infected monocytes and 12hpi-144hpi infected monocytes. ISGs are highlighted in bold. Z-scores of the log of the expression values are shown.
Extended Data Fig. 3	Features of single infected MDMs and BAL cells	Schwartz_ED_Fig3.jpg	**a**. Projection of 283 mock-infected monocytes and MDMs at 5 hpi colored by cell type. **b**. Projections as in **a**, colored by the expression level of macrophage differentiation genes. **c**. Levels of viral reads versus GFP reads in single HCMV-GFP infected MDMs. **d.** Projection of 21,839 HCMV-infected BAL cells from

			20 and 72 hpi colored by time post infection. Analysis was performed based on both cellular and viral transcripts. **e.** Projection as in d, colored by percentage of viral reads per cell. **f.** Projection as in d, colored by cell identity annotation based on reference datasets [16].
Extended Data Fig. 4	High expression of viral immediate early genes characterizes early productive MDMs.	Schwartz_ED_Fig4.jpg	**a**. Projection of HCMV-GFP infected MDMs at 5-144 hpi, analyzed based solely on cellular transcripts and colored by cluster assignment. **b**. Cluster assignment of each BAL myeloid cell according to analysis based on both viral and cellular genes (left) or on analysis based solely on cellular genes (right). Each cell is represented by a single line. The different non-productive cell clusters are colored in blue colors. Productively infected cells and clusters are colored in red. **c**. Relative expression levels, in the different MDM clusters, of viral genes from temporal classes 3-7 based on [15].
Extended Data Fig. 5	Ectopic expression of IE genes in THP1 derived macrophages drives productive infection.	Schwartz_ED_Fig5.jpg	**a**. Flow cytometry analysis of THP1 derived macrophages (DMs) infected with HCMV-GFP. Analysis was performed at 3dpi. Blue and red gates mark the GFP-dim and GFP-bright populations, respectively. **b**. ddPCR results of GFP-dim and GFP-bright HCMV-GFP infected THP1 DMs at 4 dpi. Upper panel shows detection of viral DNA, lower panel reflects detection of cellular genomes. The magenta line marks the threshold. **c**. ddPCR measurements of viral genomes from FACS-sorted GFP-bright and GFP-dim HCMV-GFP infected THP1 DMs at different times post infection. Graph is a representative of two biological replicates and shows the mean and 95% CV of poisson distribution of >10,000 PCR droplets. **d**. Measurements of infectious virus in supernatants

			from FACS-sorted GFP-bright and GFP-dim HCMV-GFP infected MDMs, at 5dpi. Points show measurements of biological replicates. p-value as calculated by one-tailed t-test on the replicates, is indicated. **e**. IE1/IE2 and mCherry protein levels at 8hpi visualized by western blot in THP1 DMs ectopically expressing UL123, UL122 or mCherry as control. GAPDH is shown as loading control. Shown is a representative of two biological replicates with similar results. **f**. pp28 (pUL99) and mCherry protein levels at 8hpi visualized by western blot in infected THP1 DMs ectopically expressing UL99 or mCherry as control. GAPDH is shown as loading control. mCherry blot is from the same samples run on a different gel. Shown is a representative of two biological replicates with similar results. **g**. Percentage of productively infected cells in infected THP1 DMs ectopically expressing mCherry (control), UL123, UL122 or UL99. Points show measurement of biological replicates. p-values as calculated by two-sided t-test on the replicates are indicated. **h**. Measurements of infectious virus in supernatants from THP1 DMs ectopically expressing UL123, UL122 or mCherry as control, at 8dpi. Points show measurements of biological replicates. p-values as calculated by one-tailed t-test on the replicates, are indicated. **i**. Percentage of productively infected cells in infected PMA-treated Kasumi-3 ectopically expressing UL123 or mCherry as control. Points show measurement of biological replicates. p-values as calculated by one-tailed t-test on the replicates are indicated. **j**. Distribution of the Spearman correlation coefficients between cellular transcript levels and viral gene expression level (left panels) or UL123 and UL122 expression levels (right panels), in

			early HCMV-GFP infected MDMs from 5hpi (top panels) or 12 hpi (bottom panels). The black line marks the matching normal distribution.
Extended Data Fig. 6	Induction of ISGs does not dictate infection outcome.	Schwartz_ED_Fig6.eps	**a**. Heatmap depicting the 40 most significantly increased genes in non-productive MDMs compared to early MDMs. ISGs are highlighted in bold. Z-scores of the log of the expression values are shown. **b**. Viral gene expression level versus ISG expression level in single HCMV-infected fibroblasts at different times post infection. Data taken from [20]. The percentage of each group of cells in the given time point is indicated. **c.** Percentage of productively infected MDMs either untreated (HCMV), or treated with interferons at the time of infection (HCMV+IFN). Points show measurements of biological replicates. p-value of the decrease in productively infected MDMs following interferon treatment, as calculated by one-tailed t-test on the replicates, is indicated. **d.** Relative expression level of representative ISGs, measured by qPCR, in infected MDMs either untreated (HCMV) or treated with interferons at the time of infection (HCMV+IFN), at 8 and 24 hpi. Points show measurements of biological replicates. p-values as calculated by one-tailed t-test on the replicates are indicated. **e.** Percentage of productively infected fibroblasts either untreated (HCMV), or treated with interferons at the time of infection (HCMV+IFN). Points show measurements of biological replicates. p-value of the decrease in productively infected fibroblasts following interferon treatment, as calculated by one-tailed t-test on the replicates, is indicated.

Extended Data Fig. 7	Intrinsic ISG levels affect HCMV infection outcome.	Schwartz_ED_Fig7.jpg	**a.** ISG expression level versus differentiation status in single bone marrow human haematopoietic stem cells. Data taken from [25] shows differentiation trajectory from hematopoietic stem cells (HSCs) to monocytes (mono, left panel) and data from [24] shows differentiation trajectory from hematopoietic stem cells (HSCs) to hematopoietic progenitor cells (HPCs, right panel). The linear regression line with confidence interval is shown. **b.** Percentage of productively infected MDMs either untreated (HCMV), or treated with interferons 24 hours prior to infection (IFN-HCMV). Points show measurements of biological replicates. p-value of the decrease in productively infected MDMs following interferon treatment, as calculated by one-tailed t-test on the replicates, is indicated. **c.** Percentage of productively infected fibroblasts either untreated (HCMV), or treated with interferons 24 hours prior to infection (IFN-HCMV). Points show measurements of biological replicates. p-value of the decrease in productively infected fibroblasts following interferon treatment, as calculated by one-tailed t-test on the replicates, is indicated. **d.** Measurements of infectious virus in supernatants from infected MDMs either untreated or treated with interferons 24 hours prior to infection, at different times post infection. **e**. qPCR measurements of viral genomes from infected MDMs either untreated or treated with interferons 24 hours prior to infection, at different times post infection. The plot shows the mean of 2 independent biological replicates. **f.** Relative expression level of representative ISGs, measured by qPCR, in infected MDMs either untreated (HCMV) or treated with ruxolitinib 24 hours prior to infection (Ruxo-HCMV), at 12 hpi.

			Points show measurements of biological replicates. p-values as calculated by one-tailed t-test on the replicates are indicated. **g**. Percentage of productively infected MDMs either untreated (HCMV), or treated with ruxolitinib 24 hours prior to infection (Ruxo-HCMV). Points show measurements of biological replicates. p-value of the increase in productively infected MDMs following Ruxo treatment, as calculated by one-tailed t-test on the replicates, is indicated. **h**. IRF9 or STAT2 protein levels as measured by western blot in THP1 DMs following CRISPR KO of IRF9 or STAT2, respectively. KO using two different gRNAs for each gene are shown. Actin was used as loading control. Shown is a representative of two biological replicates with similar results. **i.** Percentage of productively infected THP1 DMs following CRISPR KO of a control gene, IRF9 or STAT2. Two independent gRNAs were used for IRF9 and STAT2. Points show measurements of biological replicates. p-value of IRF9 or STAT2 KO compared to the control, as calculated by one-tailed t-test on the replicates is indicated. **j.** Percentage of productively infected THP1 DMs either untreated (HCMV) or treated with ruxolitinib at the time of infection (HCMV+Ruxo) following CRISPR KO of a control gene or IRF9. Points show measurements of biological replicates. p-value of IRF9 KO compared to the control, as calculated by one-tailed t-test on the replicates, is indicated.
Extended Data Fig. 8	Effects of HCMV infection on macrophage cell identity.	Schwartz_ED_Fig8.jpg	**a**. Gene set enrichment analysis (GSEA) of differentially expressed genes between GFP-dim and GFP-bright BAL infected macrophages compared to mock-infected cells, on innate immunity, immune signaling and immune identity and function pathways. **b.** Gating strategy used to determine the

			single-cell population for flow cytometry analysis of CD11b surface levels. **c.** Flow cytometry of CD11b surface levels in unstained and stained HCMV-GFP infected MDMs. **d.** Flow cytometry of CD11b surface levels in HCMV-GFP infected PMA-induced MDMs. The blue and red gates mark the non-productive and productive MDMs, respectively, as measured by GFP level. The inset in the bottom left shows the distribution of CD11b levels in the two populations. p value of the decrease in the mean fluorescence intensity in GFP-bright MDMs on the measured single cells is calculated using one-tailed t-test. Representative of two independent replicates is shown. **e.** Gating strategy used to determine the single-cell population for flow cytometry analysis of phagocytosis. **f.** Percentage of phagocytosing GFP-dim and GFP-bright HCMV-GFP infected M-CSF-induced MDMs. Points show measurements of biological replicates. p-value as calculated by t-test on the replicates is indicated.
Extended Data Fig. 9	Non-productive MDMs continuously express viral transcripts and can reactivate.	Schwartz_ED_Fig9.jpg	**a**. Heatmap depicting absolute levels of viral transcripts, in reads per million, in productive MDMs. Staging of the cells and ordering of the viral genes are as in Fig. 6a. The expression levels in the heatmap are relative to the highest level of each transcript. **b**. Percentage of viral reads in single monocytes along infection. Box plot shows standard parameters (median, Q1-Q3, 1.5 IQR). p-value as calculated by one-tailed Wilcoxon test comparing the cells in the first and last groups is indicated. n is 141, 27, 210, 348 cells for 24hpi, 48hpi, 72hpi and 144hpi, respectively. **c**. Percentage of viral reads in single non-productive PMA-induced MDMs along infection. Box plot shows standard parameters (median, Q1-Q3, 1.5 IQR). Data

			from 72 hpi and 144 hpi is from scRNA-seq of only GFP-dim cells to avoid noise coming from GFP-bright cells, expressing high levels of viral transcripts. p-value as calculated by one-tailed Wilcoxon test comparing the cells in the first and last groups is indicated. n is 413, 552, 628 cells for 24hpi, 72hpi and 144hpi, respectively. **d**. Phase-contrast and GFP microscopy images of PMA-induced MDMs infected with HCMV-GFP at different days post infection. Scale bars are 200µm. Shown are representatives of two biological replicates. **e.** Plaques formed on fibroblasts co-cultured with reactivated M-CSF-induced MDMs. Reactivation was done by either PMA or LPS treatment. Scale bars are 500µm. Shown are representatives of five and three biological replicates for PMA or LPS treatments, respectively. **f**. Plaques formed on fibroblasts co-cultured with reactivated PMA-induced MDMs. Reactivation was done by either PMA or LPS treatment. Scale bars are 500µm. Shown are representatives of two biological replicates. **g**. Plaques formed on fibroblasts co-cultured with reactivated interferon-pre treated, PMA-induced MDMs. Reactivation was done by PMA. Scale bar is 500µm. Shown is a representative of three biological replicates.
Choose an item.			

2

Item	Present?	Filename Whole original file name including extension. i.e.:	A brief, numerical description of file contents. i.e.: *Supplementary Figures 1-4, Supplementary Discussion, and Supplementary Tables 1-4.*

		Smith_SI.pdf. The extension must be .pdf	
Supplementary Information	Yes	Supplementary Table 1	Supplementary Table 1
Reporting Summary	Yes	Schwartz_reporting_summary	
Peer Review Information	No	*OFFICE USE ONLY*	

3

4

5

6

Type	Number Each type of file (Table, Video, etc.) should be numbered from 1 onwards. Multiple files of the same type should be listed in sequence, i.e.: Supplementary Video 1, Supplementary Video 2, etc.	Filename Whole original file name including extension. i.e.: *Smith_ Supplementary_Video_1.mov*	Legend or Descriptive Caption Describe the contents of the file
Choose an item.			
Choose an item.			
Choose an item.			
Choose an item.			
Choose an item.			

Choose an item.			

7

Parent Figure or Table	Filename Whole original file name including extension. i.e.: *Smith_SourceData_Fig1.xls,* or *Smith_ Unmodified_Gels_Fig1.pdf*	Data description i.e.: Unprocessed western Blots and/or gels, Statistical Source Data, etc.
Source Data Fig. 1		
Source Data Fig. 2		
Source Data Fig. 3		
Source Data Fig. 4		
Source Data Fig. 5		
Source Data Fig. 6		
Source Data Fig. 7		
Source Data Fig. 8		
Source Data Extended Data Fig./Table 1		
Source Data Extended Data Fig./Table 2		
Source Data Extended Data Fig./Table 3		

Source Data Extended Data Fig./Table 4	Schwartz_SourceData_ED_Fig4	Unprocessed western Blots
Source Data Extended Data Fig./Table 5		
Source Data Extended Data Fig./Table 6		
Source Data Extended Data Fig./Table 7	Schwartz_SourceData_ED_Fig7	Unprocessed western Blots
Source Data Extended Data Fig./Table 8		
Source Data Extended Data Fig./Table 9		
Source Data Extended Data Fig./Table 10		

8

Molecular characterization of human cytomegalovirus infection with single cell transcriptomics

Michal Schwartz[1,4*], Miri Shnayder[1,4], Aharon Nachshon[1], Tamar Arazi[1], Yaarit Kitsberg[1], Roi Levi Samia[1], Michael Lavi[1], Rottem Kuint[2], Reuven Tsabari[3], Noam Stern-Ginossar[1*]

1 Department of Molecular Genetics, Weizmann Institute of Science, Rehovot, Israel.

2 Institute of Pulmonary Medicine, Hadassah Hebrew University Medical Center, Faculty of Medicine, Hebrew University, Jerusalem, Israel.

3 Pediatric Pulmonology and CF Unit, Department of Pediatrics, Hadassah Hebrew University Medical Center, Jerusalem, Israel.

4 These authors contributed equally to this work.

* To whom correspondence should be addressed: michalsc@weizmann.ac.il or noam.stern-ginossar@weizmann.ac.il

Abstract

Human cytomegalovirus (HCMV) can result in either productive or non-productive infection, with the latter potentially leading to viral latency. The molecular factors dictating these outcomes are poorly understood. Here we used single cell transcriptomics to analyse HCMV infection progression in monocytes, which are latently infected, and macrophages, considered to be permissive for productive infection. We show that early viral gene expression levels, specifically of those encoding immediate early proteins, IE1 and IE2, are a major factor dictating productive infection. We also revealed that intrinsic, not induced, host cell interferon stimulated gene (ISG) expression level is a main determinant of infection outcome. Intrinsic ISG expression is downregulated with monocyte to macrophage differentiation, partially explaining increased macrophage susceptibility to productive HCMV infection. Furthermore, non-productive macrophages could reactivate, making them potential latent virus reservoirs. Overall, we decipher molecular features underlying HCMV infection outcomes and propose macrophages as a potential HCMV reservoir.

38 **Introduction**

39 Human cytomegalovirus (HCMV) is a prevalent pathogen of the beta-herpesvirus family,
40 infecting the majority of the human population [1]. HCMV establishes latent infection which can
41 lead to disease and mortality upon reactivation.

42 A wide range of cell types can be infected [2], but with variable infection outcomes, and generally
43 differentiated cells are more permissive. Cells from the myeloid lineage are thought to play a
44 critical role in HCMV latency and reactivation. Hematopoietic stem cells (HSCs), granulocyte-
45 macrophage progenitor (GMPs) and blood monocytes are infected with HCMV but do not
46 support productive infection and are the main cells in which HCMV latency has been
47 characterized [3–5]. While bone marrow HSCs have been proposed as the long term HCMV latent
48 reservoir, clinical data strongly implies that there are additional uncharacterized sources of
49 latent HCMV outside the bone marrow, likely within tissues [6,7]. Unlike monocytes and earlier
50 myeloid progenitors, terminally differentiated macrophages and dendritic cells were shown to
51 be permissive for productive HCMV infection [8,9] yet the molecular basis for the different
52 infection outcome between monocytes and their differentiated counterparts is not well
53 understood.

54 To shed light on molecular determinants that dictate infection outcome, we scrutinized HCMV
55 infection progression in monocytes and macrophages by single-cell RNAseq. First, we reveal that
56 macrophages can support both productive and non-productive infection. By comparing these
57 two infection outcomes, as well as to infected monocytes, we show that high early viral gene
58 expression levels, particularly of immediate early genes, facilitate productive infection. On the
59 host side, we demonstrate that intrinsic Interferon-stimulated gene (ISG) expression levels, but
60 not their induction upon infection, have a substantial effect on infection outcome and are
61 correlated to cellular differentiation. Finally, we show that non-productive macrophages can
62 reactivate to produce infectious progeny. Altogether, our findings define determinants of HCMV
63 infection outcome in the myeloid lineage and raise the possibility that macrophages serve as
64 latent viral tissue reservoirs.

65 **Results**

66 **Experimental system for studying HCMV infection outcome**

67 We initially compared infection of monocytes to differentiated monocytes by using three
68 treatments: phorbol-myristate (PMA), GM-CSF/IL-4 and M-CSF, which have all been shown to
69 trigger monocyte differentiation [10,11]. We used an HCMV TB40-E strain containing an SV40-GFP
70 reporter [12], which allows quantification of productive infection efficiency. As expected, 3 days
71 post infection (dpi) in monocytes, almost all of the cells show a small increase in GFP, indicating
72 they are infected but that viral gene expression is repressed (Fig. 1a and Extended Data Fig. 1a).
73 Following all differentiation-inducing treatments, infection resulted in two distinct populations:
74 GFP-dim, suggesting the cells were infected but viral gene expression is repressed, and GFP-
75 bright, suggesting productive infection (Fig. 1a and Extended Data Fig. 1b-c). Cells within each of
76 the treatments displayed uniform shifts in surface expression of macrophage/dendritic cell
77 markers, negating the possibility that differences in differentiation efficiency within the cell
78 populations can solely explain the differences in infection outcomes (Extended Data Fig. 1d). For
79 further experiments we primarily used PMA derived macrophages because they are commonly
80 used in HCMV studies and exhibited a large and distinct population of GFP-bright cells (Fig. 1a).
81 The two distinct populations in infected monocyte-derived macrophages (MDMs) are not
82 apparent at early stages of infection(Extended Data Fig. 1e), suggesting that they likely do not
83 reflect two separate initial populations, but rather two different infection outcomes . Infection
84 of MDMs, but not of monocytes, resulted in production of infectious virions (Extended Data Fig.
85 1f), confirming productive infection in these cells.

86 We verified that the GFP-dim and GFP-bright populations reflect different infection outcomes,
87 by showing that GFP-bright cells are larger compared to GFP-dim cells (Extended Data Fig. 1g-h),
88 a known feature of lytic HCMV infection. Moreover, both sorted GFP-bright and GFP-dim
89 populations (Extended Data Fig. 1i) harbored viral DNA, however, at 4dpi viral DNA load was
90 much higher in the GFP-bright cells (Extended Data Fig. 1j-l) and substantially increased with
91 time in the GFP-bright but not in the GFP-dim population (Fig. 1b). This indicates that viral
92 genome replication occurs only in the GFP-bright population. In addition, GFP-bright MDMs
93 produce infectious virions while GFP-dim cells do not (Fig. 1c). These results indicate that the
94 majority of MDMs were infected with the virus but a productive infection only developed in
95 some of the cells. We further assessed infection of natural tissue myeloid cells, collected from

96 BronchoAlveolar Lavage (BAL) samples. The presence of macrophages in these samples was
97 verified by size, morphology and surface marker staining (Extended Data Fig. 1m-n). Indeed, also
98 in BAL macrophages we observed two distinct populations of GFP-dim and GFP-bright cells that
99 differ in viral genome levels (Fig. 1d-e and Extended Data Fig. 1o).

100

101 **Single-cell RNA-seq of HCMV-infected monocytes and MDMs**

102 To shed light on the processes governing these two infection outcomes, we analyzed infected
103 monocytes and PMA-induced MDMs from the same donor at 5, 12, 24, 48, 72 and 144 hours
104 post infection (hpi), as well as mock-infected monocytes and MDMs at the 5 and 144 hpi time
105 points, by single-cell RNA-sequencing (scRNA-seq, Fig. 1f). Projection of all cells according to
106 both cellular and viral reads, revealed several distinct groups of cells (Fig. 1g, Extended Data Fig.
107 2a). At 5 hpi, infected monocytes were grouped with mock-infected monocytes (Fig. 1g,
108 Extended Data Fig. 2a). Infected monocytes from 12 hpi onwards appeared as a single
109 population (Fig.1g) and stratified from early monocytes mainly based on interferon stimulated
110 genes (ISGs, Extended Data Fig. 2b). As expected, viral transcript load in infected monocytes
111 remained low in all cells along infection (median=0.063%, Fig. 1h), indicating lack of productive
112 infection [13–15]. In contrast, infected MDMs from 24 hpi and onwards, were separated into two
113 distinct populations (Fig. 1g) differing in viral transcript load, reflecting two infection outcomes:
114 productive, in which viral transcript load increased as infection progressed, and non-productive,
115 in which viral transcript loads were low (median=0.226%, Fig. 1h). MDMs from earlier time
116 points clustered with mock-infected MDMs (Fig. 1g, Extended Data 2a), suggesting milder
117 transcriptional changes relative to later in infection.

118

119 **Two distinct infection outcomes in infected macrophages**

120 Since infection of MDMs results in non-productive and productive outcomes, we focused our
121 analysis on infected MDMs. Notably, all mock-infected MDMs were transcriptionally distinct
122 from the initial monocyte population (Extended Data Fig. 3a) and showed increased macrophage
123 differentiation signature (Extended Data Fig. 3b) indicating that it is unlikely that the two distinct
124 infection outcomes originate from two initially distinct populations. Projection of all infected
125 MDMs according to cellular and viral transcripts, revealed that cells were divided into three

126 discernible populations (Fig. 2a). Most of the cells from the early time points (5-12 hpi) belong
127 to a single group, harboring low levels of viral transcripts and indistinguishable in regard to
128 infection outcome, while cells from later time points in infection split into two additional distinct
129 groups (Fig. 2b), which differ greatly in the level of viral transcripts (Fig. 2c-d) and in virally
130 encoded GFP expression levels (Extended Data Fig. 3c). The three main populations therefore
131 correspond to early, non-productive, and productive MDMs (Fig 2e). Further sub-clustering
132 corresponds to progression in the given trajectory with time post infection (Fig. 2b, e).

133 scRNA-seq analysis of infected BAL cells from 20 and 72hpi demonstrated that the cells stratify
134 into two distinct populations and an additional small population that expresses significantly
135 higher viral transcript levels, reflecting productively infected cells (Extended Data Fig. 3d-e). By
136 using an annotated reference dataset [16], we found that these two populations correspond to
137 lymphocytes, mostly T cells, and to myeloid cells, mostly macrophages, and the productive cells
138 originate from myeloid cells (Extended Data Fig. 3f). Analysis of the myeloid cells demonstrated
139 that infection of natural tissue macrophages also results in two outcomes: productive and non-
140 productive, as reflected by high and low viral transcript levels, respectively (Fig. 2f).

141

142 **Viral IE gene expression determines infection outcome**

143 To delineate the contribution of cellular and viral genes to the stratification of the MDMs into
144 distinct groups (early, non-productive, productive), we next analyzed the transcriptome solely
145 according to cellular genes. This analysis produced the same three distinct groups of cells and
146 very similar cluster stratification, indicating these three infection states are associated with
147 corresponding changes in the cellular transcriptome (Fig. 3a and Extended Data Fig. 4a). There
148 were two exceptions: Cluster 5, which includes very few non-productive cells from different
149 time points, and cluster 7, which is the earliest productive cluster (Fig. 2a) and when clustering
150 was based only on cellular genes, these cells clustered together with the early cells (Fig. 3a).
151 This demonstrates that the first major transcriptional signature that defines cells as productively
152 infected is robust viral gene expression, and this was also apparent in analysis of infected BAL
153 macrophages (Extended Data Fig. 4b). Quantification of the expression of the different temporal
154 classes of viral genes[15] within cells in the different clusters, reveals that in the early productive
155 cells, compared to their non-productive counterparts, there is high relative expression of

156 immediate early (IE) genes, as well as specific induction of true early genes, but not of other viral
157 temporal classes (Fig. 3b, Extended Data Fig. 4c). This suggests that expression of IE genes at
158 early stages of infection, at levels sufficient to induce early genes, has a major role in dictating
159 infection outcome. Indeed, the UL123 and UL122 transcripts which encode the major IE genes,
160 IE1 and IE2, respectively, are specifically expressed in early productive cells (Fig. 3c). We further
161 scrutinized the effect of IE gene expression on infection outcome, in macrophages derived from
162 the monocytic cell line THP1, whose infection similarly exhibits two outcomes (Extended Data
163 Fig. 5a-d). Induced ectopic expression of either UL123 or UL122 but not of a control gene
164 (mCherry) or UL99, a viral late gene (Extended Data Fig. 5e-f), significantly increased the
165 percentage of productively infected cells (Fig. 3d and Extended Data Fig. 5g). Moreover, ectopic
166 expression of both IE genes, increased the production of infectious progeny (Extended Data Fig.
167 5h). The effect of IE1 was further validated in differentiated Kasumi-3 cells (Extended Fig. 5i).

168 Since scRNA-seq gives unprecedented detail on inter-cellular heterogeneity, we next explored
169 whether we can identify cellular genes that correlate with the initial levels of viral gene
170 expression but we could not detect any significant association (Extended Data Fig. 5j). This likely
171 reflects the relatively homogenous nature of the cells we used, such that small differences in
172 gene expression are masked by other factors, such as the amount of incoming virions [17], or
173 variability between the content of virions [18].

174

175 **Induction of ISGs does not dictate infection outcome**

176 We next examined the features that characterize the shift from early infection to the non-
177 productive population. The genes that were most upregulated in the non-productive cells were
178 ISGs (Extended Data Fig. 6a, Fig. 4a-b). Analysis of ISG expression versus viral gene expression in
179 infected MDMs revealed that at early time points, both viral gene and ISG expression are low. As
180 infection progressed, most of the cells increased either viral gene expression or ISG expression
181 (Fig. 4c). Notably, the cells of both trajectories were exposed to the same extracellular signals
182 (e.g. interferons), as they were grown together in the same culture dish, indicating that the
183 induction of viral gene expression renders the cells unresponsive to interferon signaling [19]. Since
184 we hardly detected infected MDMs that induced both viral genes and ISGs, this analysis may
185 imply that these events describe two competing deterministic outcomes - induction of viral

genes resulting in productive infection, or induction of ISGs prohibiting productive infection. However, analysis of the percentage of cells in the different populations at each time point indicates that productive cells likely also originate from the non-productive groups in which ISGs were already induced, as the percentage of productive cells reaches numbers that cannot be solely explained by transition from the early infected population (Fig. 4d). This therefore suggests that induction of interferon response does not forestall establishment of productive infection and the main determinant that governs infection outcome is the induction of viral gene expression above a certain threshold. Analysis of a recent single cell RNA-seq dataset along HCMV infection of fibroblasts [20] demonstrated the same phenomenon (Extended Data Fig. 6b). These observations suggest that induction of ISGs by an infected cell does not deterministically prevent the establishment of productive infection within that cell.

In accordance with these results, adding interferon at the time of infection did not affect the percentage of productively infected cells (Fig. 4e and Extended Data Fig. 6c), despite significant increase in ISG expression (Extended Data Fig 6d). Similar results were obtained in low MOI infection of fibroblasts (Fig. 4f and Extended Data Fig. 6e). Together these results demonstrate that activation of ISGs in response to infection may slow productive infection but overall does not deterministically prevent it.

Intrinsic ISG levels affect HCMV infection outcome

Analysis of monocytes compared to non-productive MDMs showed similarly low viral gene expression but higher ISG expression level even at the earliest infection stage (Fig. 4g). Further analysis of mock-infected monocytes, MDMs and fibroblasts[20] revealed that intrinsic levels of ISGs (in mock-infected cells) in fibroblasts is lower than in MDMs, which in turn is lower than in monocytes (Fig. 4h) and there is an inverse-correlation between intrinsic ISG levels and viral gene expression levels at early stages of infection (Fig. 4i). Since the permissiveness for productive infection is tightly linked to differentiation state [21,22], we examined the link between intrinsic expression of ISGs and differentiation state. Indeed, intrinsic levels of many ISGs decrease along differentiation of monocytes to MDMs [23] (Fig. 4j-k) and along differentiation of hematopoietic cells in the bone marrow [24,25] (Extended Data Fig. 7a), suggesting a tight link

215 between intrinsic levels of ISGs, differentiation and permissiveness to productive HCMV
216 infection.

217 To explore if the levels of ISGs at the time of infection affect infection outcome, we tested the
218 effect of interferon pre-treatment on HCMV infection. Addition of interferons 24 hours prior to
219 infection of MDMs or fibroblasts eliminated productive infection (Fig. 4e-f, Extended Fig. 7b-d),
220 blocked viral DNA replication (Extended Data Fig. 7e), and led to reduction in viral gene
221 expression already at 12hpi (Fig. 4l). These results indicate that ISGs act to block the virus at the
222 stage of immediate early viral gene expression or earlier.

223 We next sought to test whether reducing intrinsic ISG levels would indeed affect infection
224 outcome. Intrinsic levels of ISGs may originate from low basal levels of interferon signaling,
225 however pretreatment of MDMs with ruxolitinib, a potent and selective Janus kinase (JAK) 1 and
226 2 inhibitor did not affect the intrinsic levels of ISGs (Extended Data Fig. 7f) and correspondingly
227 did not affect infection outcome (Extended Data Fig. 7g). It was recently suggested that basal
228 expression of ISGs is controlled by preformed STAT2-IRF9 complexes, independent of interferon
229 receptor signaling [26]. Indeed, depletion of IRF9 or STAT2 using CRISPR-cas9 in THP1 derived
230 macrophages (Extended Data Fig. 7h) reduced the intrinsic expression of many ISGs (Fig. 4m)
231 and led to an increase in the percentage of productively infected cells (Fig. 4n and Extended
232 Data Fig. 7i). This effect was not diminished by addition of ruxolitinib at the time of infection
233 (Extended Data Fig. 7j), illustrating it is due to reduction in intrinsic ISGs rather than reduced
234 induction of ISGs following infection. Overall, these results indicate that intrinsic expression of
235 ISGs, which decrease upon differentiation, plays a major role in dictating HCMV infection
236 outcome.

237

238 **Productive HCMV infection disrupts macrophage identity**

239 We next analyzed cellular transcriptional changes and revealed that several pathways known to
240 be modulated during HCMV infection in fibroblasts were significantly enriched in productive
241 MDMs, including metabolism, cell cycle and translation pathways (Fig. 5a)[27,28]. As mentioned
242 above, non-productive MDMs significantly induced, mainly and most robustly, ISGs.

243 Several pathways were suppressed in productive MDMs, including some which are associated
244 with immune signaling or common functions of macrophages, such as antigen presentation and

245 phagocytosis as well as genes related to hematopoietic cell lineage (Fig. 5a). RNA-seq on
246 infected BAL macrophages showed that indeed similar pathways related to immune signaling
247 and macrophage identity are significantly suppressed in productively infected BAL macrophages
248 and ISGs are strongly induced in the non-productively infected macrophages (Extended Data Fig.
249 8a). The disruption of macrophage identity and function was further supported by reduction in
250 surface levels of CD11b, a prominent macrophage marker, in productively infected MDMs,
251 induced by either PMA or M-CSF, (Fig. 5b and Extended Data Fig. 8b-d) as well as reduced
252 phagocytosis activity in these cells (Fig. 5c and Extended Data Fig. 8e-f). These results show,
253 both on the transcriptional and the functional levels, that productive HCMV infection disrupts
254 macrophage identity and function.

255 **Viral gene expression in HCMV infected MDMs**

256 We next examined viral gene temporal expression along productive and non-productive
257 infection. For the productive MDMs we binned the cells according to % viral reads to reflect
258 progression along infection. This was followed by hierarchical clustering, revealing a temporal
259 expression cascade in productive MDMs that is similar to that seen in infection of fibroblasts [15]
260 (Fig. 6a, left heatmap). This analysis reflects relative expression patterns, i.e. how each viral
261 gene is expressed relative to all other viral genes. At the absolute level, almost all viral genes
262 increase in their expression levels as infection progresses (Extended Data Fig. 9a). In non-
263 productive MDMs, despite viral transcript levels being low throughout infection, they slightly
264 increase with time (Fig. 6b), unlike infected monocytes (Extended Data Fig. 9b) [13]. To exclude the
265 possibility that this apparent increase in viral reads originates from low level cross
266 contamination from productive cells, we conducted another experiment in which at 72 and 144
267 hpi only GFP-dim cells were processed, which further demonstrated a small increase in viral
268 transcript levels (Extended Data Fig. 9c). Nevertheless, analysis of viral gene expression in non-
269 productive cells along infection revealed broad gene expression with no clear kinetic program
270 (Fig. 6a, right heatmap).

271

272 **Non-productive MDMs reactivate and release infectious virus**

273 The observation that viral gene expression is maintained at higher levels in non-productive
274 macrophages compared to monocytes, indicates a less repressed state in the former.

275 Furthermore, in culture, these cells survived for relatively long periods (Extended Data Fig. 9d)
276 and also *in-vivo* macrophages can be long lived cells [29]. We therefore tested if the virus residing
277 in non-productive MDMs, differentiated either by PMA or M-CSF, could reactivate. We did not
278 observe any spontaneous reactivation, however, additional stimulation with either PMA or LPS
279 at 7dpi resulted in reactivation and release of infectious virus, (Fig. 6c, Extended Data Fig. 9e-f).
280 Moreover, interferon-pretreated, infected MDMs, which, as described above, are non-
281 productively infected, also reactivated when PMA was added at 7dpi, and released infectious
282 virus (Fig. 6d and Extended Data Fig. 9g). It is noteworthy that in these cells there was some low
283 level reactivation in the absence of additional stimuli, which is in line with previous findings [30].

284 These results indicate that in cell culture, macrophages can be infected in a latent-like manner,
285 in which viral gene expression is repressed, but the viral genome retains the ability to reactivate
286 upon additional stimulation. HCMV infection following exposure to interferons may further lead
287 to a similar latent-like infection that can also result in reactivation.

288 **Discussion**

289 HCMV infection can result in different outcomes: productive infection leading to release of
290 infectious virus, or non-productive infection, potentially leading to latency establishment, from
291 which the virus can later reactivate. To identify, in an unbiased manner, determinants of HCMV
292 infection outcome, we analyzed the progression of HCMV infection in monocytes and
293 macrophages, which support latent and lytic infection, respectively. Our data demonstrates that
294 in fact, HCMV infection of monocyte-derived macrophages (MDMs) can be either productive or
295 non-productive, allowing us to analyze the decision point of infection outcome. We show that
296 the unequivocal factor associated with the earliest split of productive cells, is viral gene
297 expression and specifically the expression of immediate early genes and the onset of early gene
298 expression. The importance of IE gene expression was already acknowledged in the past [31],
299 however, ectopic expression of these genes in THP1 cells was previously shown to be
300 insufficient to induce productive infection [32]. Here we show that overexpression of UL123 or
301 UL122 in THP1-derived macrophages shifts infected cells towards productive infection. The
302 notable difference between the reports is the use of differentiated versus non-differentiated
303 THP1 cells. Further research is needed in order to uncover what are the additional barriers in
304 non-differentiated THP1 cells and whether they extend to primary monocytes. The lack of a
305 clear cellular gene expression signature that is associated with viral gene expression levels at the
306 early stages of infection, indicates that in this experimental set-up, infection outcome is likely
307 determined primarily by the amount of infectious virus entering the cell [17], which will have
308 significant consequences on the initial induction of viral gene transcription.
309 The defining signature of non-productive MDMs is the expression of ISGs as was also shown in
310 HSV-1 infected cells [33]. However, our data suggests that induction of ISGs following infection
311 does not deterministically define infection outcome, although it does not rule out the possibility
312 that it slows down or hampers the propagation of the virus.

313 Instead, we reveal that intrinsic expression levels of ISGs prior to infection dictate infection
314 outcome, and are associated with myeloid differentiation state. This connection between
315 intrinsic expression of ISGs, differentiation and infection was noted previously for infection of
316 embryonic stem cells with several RNA viruses [34]. Our results suggest that this link could be a
317 major contributing factor to the cell-type dependent infection outcome of HCMV and potentially
318 other herpesviruses.

319 Beyond explaining cell type differences, this effect of intrinsic levels of ISGs could be relevant to
320 the establishment of latency. In a setting where not all cells are infected, induction of
321 interferons by infected cells could shift the fate of neighboring uninfected cells towards non-
322 productive infection, potentially aiding the virus to seed latent reservoirs, and perhaps also
323 prolonging infection in case of viral gene silencing which can be reversed [30].

324 Reactivation of HCMV from latency is a substantial clinical burden in immunocompromised
325 individuals and may cause serious and often life-threatening disease [35]. The only characterized
326 HCMV latent reservoir to date is the bone marrow HSCs [36], however, clinical data suggest that
327 latent reservoirs exist also in tissues [7]. For many years tissue resident macrophages were
328 considered to be short lived and be replenished regularly by circulating monocytes. However,
329 mounting evidence indicates that resident macrophage populations reside in organs and can
330 remain for years [29,37,38]. Our results demonstrate that macrophages have the potential to be
331 infected in a latent-like manner, in which they carry viral genomes, repress viral gene expression
332 and can reactivate. Natural infection of macrophages is supported by reports of HCMV
333 reactivation in alveolar macrophages from healthy HCMV carriers [39] and of latent murine
334 macrophages following clearance of an acute CMV infection [40], implying that tissue
335 macrophages may serve as latent CMV reservoir.

336 On the other hand, our analysis of productively infected macrophages demonstrates a dramatic
337 effect on macrophage identity and function. This analysis aligns with a recent study by Baasch et
338 al. that showed productive MCMV infection of macrophages reprograms macrophage identity
339 and disrupts their function, leading to higher susceptibility to secondary lung infection [41].

340 These findings highlight macrophages as prospective critical players during HCMV infection both
341 in pathogenesis at the time of acute infection, as well as potential latent reservoirs in tissues.

342 **Methods**

343 Ethics statement

344 All fresh peripheral blood samples were obtained after approval of protocols by the Weizmann
345 Institutional Review Board (IRB application 92–1) and following informed consent from the
346 donors. The study using BronchoAlveolar Lavage (BAL) fluid samples was approved by the
347 Hadassah Medical Organization research ethics committee in accordance with the Declaration of
348 Helsinki (HMO-0704-20). Written informed consent to retain BAL fluid was obtained from
349 patients undergoing bronchoscopy. Blood donors and bronchoscopy patients were not
350 compensated.

351 Cell culture and virus

352 Primary CD14+ monocytes were isolated from fresh venous blood, obtained from healthy
353 donors, males and females, aged 25-45, using Lymphoprep (Stemcell Technologies) density
354 gradient followed by magnetic cell sorting with CD14+ magnetic beads (Miltenyi Biotec).
355 Monocytes were cultured in X-Vivo15 media (Lonza) supplemented with 2.25 mM L-glutamine
356 at 37°C in 5% CO2, at a concentration of 1-2 million cells/ml in non-stick tubes to avoid
357 differentiation.

358 Where indicated, primary monocytes were treated with the following treatments immediately
359 following isolation and plating: PMA 50ng/ml for 3 days, GM-CSF and IL-4 1000U/ml each for 6
360 days with cytokine replenishing after 3 days, M-CSF 20ng/ml for 6days with cytokine
361 replenishing after 3 days, TNFα 10ng/ml for 6 days. All treatments were done in Roswell Park
362 Memorial Institute (RPMI) with 10% heat-inactivated fetal bovine serum (FBS), 2 mM L-
363 glutamine, and 100 units/ml penicillin and streptomycin (Beit-Haemek, Israel) and MDMs were
364 grown in this media following treatment. 293T cells (ATCC- CRL-3216) were maintained in
365 DMEM with 10% FBS, 2 mM L-glutamine, and 100 units/ml penicillin and streptomycin (Beit-
366 Haemek, Israel). Primary human foreskin fibroblasts (ATCC CRL-1634) were maintained in DMEM
367 with 10% FBS, 2 mM L-glutamine, and 100 units/ml penicillin and streptomycin (Beit-Haemek,
368 Israel). THP1 cells, purchased from ATCC (TIB-202), were grown in RPMI media with 15% heat-
369 inactivated fetal bovine serum (FBS), 2 mM L-glutamine, and 100 units/ml penicillin and
370 streptomycin (Beit-Haemek, Israel). Kasumi-3, purchased from ATCC (CRL-2725) were grown in
371 RPMI media with 20% heat-inactivated fetal bovine serum (FBS), 2 mM L-glutamine, and 100

372 units/ml penicillin and streptomycin (Beit-Haemek, Israel). Differentiation of THP1 and Kasumi-3
373 cells was done by adding PMA 50ng/ml for 2 days. Infection and growth following infection were
374 done in the media containing 10% FBS. Interferon treatment was done with a combination of
375 550 U/ml IFNα, 700 U/ml IFNβ and 500 U/ml IFNγ. Ruxolitinib treatment was done at a
376 concentration of 4μM.

377 BronchoAlveolar Lavage fluid was obtained from routine bronchoscopies of patients, males and
378 females aged 58-82. 15-40ml were obtained from each sample and diluted by adding an equal
379 volume of RPMI media with 10% heat-inactivated fetal bovine serum (FBS), 2 mM L-glutamine,
380 and 100 units/ml penicillin and streptomycin (Beit-Haemek, Israel). Diluted BAL fluid was
381 transferred through a 70uM filter and plated on a tissue culture dish. Adherent cells were
382 washed thoroughly prior to infection.

383 The TB40E strain of HCMV, containing an SV40-GFP tag, was described previously [12]. Virus was
384 propagated by adenofection of infectious bacterial artificial chromosome (BAC) DNA into
385 fibroblasts as was previously described [42]. Viral stocks were concentrated by centrifugation at
386 26000xg, 4°C for 120 minutes. Infectious virus yields were assayed on primary fibroblasts.

387 Infection and reactivation procedures

388 Infection was performed by incubating cells with the virus for 3 hr, washing twice and
389 supplementing with fresh media. Initial experiments with primary non-differentiated and
390 differentiated monocytes as well as the single cell experiments of monocytes and MDMs were
391 done at MOI=10 to ensure infection of all the cells. Notably, since this MOI is based on
392 quantification of infectious particles in fibroblasts it is likely effectively lower in monocytic cells.
393 The single cell experiments in BAL macrophages as well as follow up experiments in THP1- and
394 primary monocyte- derived macrophages were done in MOI=5. For reactivation assays, GFP-dim
395 infected MDMs were sorted at 4dpi and plated in 96-well plates (10,000 cells per well),
396 interferon-pretreated MDMs were used following infection without further sorting. At 7dpi cells
397 were either treated, as indicated, with 50ng/ml PMA (Sigma), or 500ng/ml LPS (Sigma) or left
398 untreated for 3 days and then the media was replaced with fresh untreated media. At 14dpi, 7
399 days post treatment, GFP positive cells were counted on a fluorescent microscope. At 18dpi
400 7500 fibroblasts per well were seeded with the MDMs and plaque formation was followed and
401 imaged for a period of 14 days.

402 Flow cytometry and sorting

403 Cells were analyzed on a BD Accuri C6 using the BD Accuri C6 software or a BD LSRII and sorted
404 on a BD FACSAria III using FACSDiva software. All analyses and figures were done with FlowJo.
405 All histograms were plotted with modal normalization.

406 Measurement of viral progeny

407 Fibroblasts were infected with known volumes of supernatants taken from infected cultures.
408 Number of GFP positive fibroblasts were measured at 2dpi by flow cytometry or microscopy and
409 the infectious particles per volume was calculated.

410 Measurement of viral genomes by digital PCR

411 DNA was extracted from cell pellets in a 1:1 mixture of lysis solutions A (100 mM KCl, 10 mM
412 Tris–HCl pH 8.3, and 2.5 mM MgCl2) and B (10 mM Tris–HCl pH 8.3, 2.5 mM MgCl2, 0.25%
413 Tween 20, 0.25% Non-idet P-40, and 0.4 mg/ml Proteinase K), for 60 min at 60˚C followed by a
414 10 min 95˚C incubation. Measurement of viral DNA was done using the QX200 droplet digital
415 PCR system (Bio-Rad), using FAM labeled HCMV primer and probe: Human CMV HHV5 kit for
416 qPCR using a glycoprotein B target (PrimerDesign); and HEX labeled RPP30 copy number assay
417 for ddPCR (Bio-Rad), as previously described [43]. Analysis was done using the Quantasoft
418 software.

419 Microscopy

420 Imaging was performed on an Olympus Ix73 inverted fluorescent microscope using a X4 or a X10
421 objective and an Olympus DP73 camera using the CellSens dimensions software or on an
422 AxioObserver Z1 wide-field microscope using a X20 objective and Axiocam 506 mono camera
423 using the ZEN software.

424 Single cell RNA sequencing library preparation

425 For primary monocytes and MDMs, single-cell sorting and library preparation were conducted
426 according to the massively parallel single-cell RNA-seq (MARS-seq) protocol, as previously
427 described [44]. In brief, single cells were FACS sorted into wells of 384-well capture plates
428 containing 2µl of lysis buffer and reverse transcription (RT)-indexed poly(T) primers, thus
429 generating libraries representing the 3’ end of mRNA transcripts. Eight empty wells were kept in

430 each 384-well plate as a no-cell control during data analysis. Immediately after sorting, each
431 plate was spun down to ensure cell immersion into the lysis solution, snap-frozen on dry ice, and
432 stored at -80°C until processed. Barcoded single-cell capture plates were prepared with a Bravo
433 automated liquid handling platform (Agilent). For generation of the RNA library, mRNA from
434 single cells was converted into cDNA in the capture plates and pooled by centrifugation to
435 VBLOCK200 reservoir (Clickbio). The pooled sample was linearly amplified by T7 in vitro
436 transcription, and the resulting RNA was fragmented and converted into a sequencing-ready
437 library by tagging the samples with pool barcodes and Illumina sequences during ligation, RT,
438 and PCR. Each pool of cells was tested for library quality, and concentration was assessed as
439 described earlier [44]. In total we analyzed 871 monocytes and 2355 MDMs. Numbers of cells in
440 clusters 1-10 of infected MDMs are: 347, 325, 232 229, 33, 122, 53, 274, 117, 83.

441 For BAL cells, pools of 10,000 cells were prepared for scRNA-seq using Chromium Single Cell 3'
442 Gene Expression v3.1 kit according to the manufacturer's instructions (10x Genomics).

443 <u>sc RNA-seq data analysis</u>

444 Analysis of MARS-seq data was done with the tools described in Jaitin et al. [45]. The reference
445 was created from the hg19 and TB40E (NCBI EF999921.1) strain of HCMV. The transcription
446 units of the virus were based on NCBI annotations, with some changes based on the alignment
447 results. This includes merging several transcripts (taking into account that the library maps only
448 the 3' ends of transcripts) and adding some antisense transcripts. Read assignment to wells was
449 based on the batch barcode (4 bp) and the well barcode (7 bp) and reads with low-quality
450 barcodes were removed. The trimmed read (37 bp) was aligned with the reference using Bowtie
451 2 [46], and the counting of the reads is done based on unique molecular identifiers (UMIs, 8 bp).
452 For each batch, the leakage noise level was estimated by comparing the number of UMIs in the
453 eight empty wells to the total number of UMIs in the batch. The noise levels in all batches was
454 lower than 1.5% . Wells with less than 500 or more than 5,000 expressed genes, or more than
455 20,000 reads were discarded. The number of wells that were used for further analysis is 3,226 .

456 For 10xGenomics data, we used Cell Ranger software (V6.1.2, 10x Genomics) with the default
457 settings to process the FASTQ files with the references used in the analysis of the MARS-seq
458 data. Cells with less than 500 or more than 10,000 expressed genes, or more than 30,000 reads
459 were discarded. The number of wells that were used for further analysis is 21,839 .

460 All single cell analyses were done using Seurat V4.0.3 [16]. To visualize single-cell datasets, we
461 performed dimension reduction by Uniform Manifold Approximation and Projection (UMAP),
462 based on both cellular and viral genes in Fig. 1, 2 and Extended Data Fig. 3 or only cellular genes
463 in Fig. 3 and Extended Data Fig. 4. Clusters of MDMs were numbered based on % viral reads in
464 the cluster, from lowest to highest. Cluster 5 includes very few non-productive cells from
465 different time points and its nature is unclear, but since it is very small, these cells were
466 removed from all following cluster-based analyses. Annotation of cell types in BAL samples was
467 done using the Azimuth application [16].

468 Calculation of viral and cellular gene expression levels in single cells

469 Expression of a single cellular gene or a group of cellular genes in single cells is calculated as the
470 percentage of reads on this gene or group of genes out of the total cellular reads in a cell. % viral
471 reads is calculated as the percentage of reads on all viral genes out of all reads in a cell. These
472 numbers were used for coloring UMAP plots in Fig. 1h, 2c, 2f, 4a Extended Data Fig. 3b, 3e and
473 for plots in Fig. 2d, 4b, 4c, 4g, 4h, 4i, 6b, Extended Data Fig. 6b, 7a, 9b, 9c. The list of ISGs is the
474 combined list of the following gene sets: Hallmark interferon alpha response, Hallmark
475 interferon gamma response and Reactome interferon signaling. The list of Macrophage
476 differentiation genes is based on the list of genes in the GO term regulation of macrophage
477 differentiation (GO:0045649).

478 Relative gene expression level of a single viral gene or a group of viral genes is calculated as the
479 percentage of reads on this gene or group of genes out of the total viral reads in a cell. These
480 numbers were used for coloring the UMAP plot in Fig. 3c and for plots in Fig. 3b, and Extended
481 Data Fig. 4c.

482 Subtraction of cross contaminating viral reads was done in the following way: for each plate the
483 level of noise was estimated from the ratio between the average number of UMIs in 8 empty
484 wells to the average number of UMIs in the plate. This number was used to calculate the
485 fraction of viral UMIs that can be attributed to leakage between cells, and was subtracted from
486 the number of viral reads in all cells of the plate.

487 Bulk RNA-seq library preparation and alignment

488 For RNA-seq of THP1 cells, cells were collected with Tri-Reagent (Sigma-Aldrich), total RNA was
489 extracted by phase separation and poly(A) selection was performed using Dynabeads mRNA

490 DIRECT Purification Kit (Invitrogen) according to the manufacturer's protocol. RNA-seq libraries
491 were generated as previously described [47]. mRNA samples of 4 ng were subjected to DNaseI
492 treatment and 3' dephosphorylation using FastAP Thermosensitive Alkaline Phosphatase
493 (Thermo Scientific) and T4 PNK (NEB) followed by 3' adaptor ligation using T4 ligase (NEB). The
494 ligated products were used for reverse transcription with SSIII (Invitrogen) for first-strand cDNA
495 synthesis. The cDNA products were 3' ligated with a second adaptor using T4 ligase and
496 amplified with 8 cycles of PCR for final library products of 200–300 base pairs. Raw sequences
497 were first trimmed at their 30 end, removing the illumina adapter and polyA tail. Alignment was
498 performed using Bowtie 1 [48] (allowing up to 2 mismatches) and reads were aligned to the
499 human (hg19). Reads aligned to ribosomal RNA were removed. Reads that were not aligned to
500 the genome were then aligned to the transcriptome.

501 For RNA-seq of BAL macrophages, pellets from cell sorting were lysed in RLT buffer (Qiagen)
502 containing 40mM DTT. Due to the low number of cells, RNA-seq libraries were performed using
503 a modified mcSCRB-seq [49] adapted for bulk RNA-seq. Briefly, RNA was isolated using SPRI beads,
504 reverse transcription and template switching was performed with indexed poly(T) primers in the
505 presence of polyethylene glycol, followed by amplification of the final library.

506 66-bp raw reads were aligned using STAR (V2.7.1) [50] to concatenation of the human (hg19) and
507 the viral genomes (NCBI EF999921.1). Counting of reads per gene was done based on unique
508 molecular identifiers (UMIs, 10 bp).

509 Plasmids and lentiviral transduction

510 UL123, UL122, UL99 or mCherry were cloned into pLVX-Puro-TetONE-SARS-CoV-2-nsp1-
511 2XStrep (kind gift from Nevan Krogan, UCSF) in place of the SARS-CoV-2-nsp1-2XStrep cassette.
512 UL123 was also cloned into pLVX-EF1alpha-SARS-CoV-2-nsp1-2XStrep-IRES-Puro (Addgene
513 plasmid #141367) in place of the SARS-CoV-2-nsp1-2XStrep cassette. The UL123, UL122, and
514 UL99 coding sequence were amplified from cDNA of HCMV infected fibroblasts with primers
515 containing flanking regions homologous to the vector (Supplementary Table 1). The mCherry
516 was amplified from an expression plasmid using primers containing flanking regions homologous
517 to the vector (Supplementary Table 1). The plasmids were amplified with the appropriate
518 primers (Supplementary Table 1). The amplified PCR fragments were cleaned using a gel
519 extraction kit (Promega) according to the manufacturer's protocol. mCherry was cloned into the

520 vector by restriction-free cloning [51] and the viral genes were cloned into the vectors using a
521 Gibson assembly protocol [52].

522 CRISPR KO was done using a CRISPR–cas9 system, with lentiCRISPR v2 plasmid (Addgene no.
523 52961). sgRNAs were cloned downstream of the U6 promoter (Supplementary Table 1).

524 Lentiviral particles were generated by co-transfection of the expression constructs and 2nd
525 generation packaging plasmids (psPAX2, Addgene#12260 & pMD2.G, Addgene#12259), using
526 jetPEI DNA transfection reagent (Polyplus transfection) into 293T cells, according to the
527 manufacturer's instructions. 60 hours post transfection, supernatants were collected and
528 filtered through a 0.45µm PVDF filter (Millex). THP1 cells were transduced with lentiviral
529 particles by spinfection (800xg, 1hr) and were then puromycin-selected (1ug/mL) for 4 days.
530 Puromycin was removed prior to subsequent differentiation. Induction of the inducible
531 transgene was done by addition of 100ng/ml Doxycycline (Sigma) 24 hours prior to HCMV
532 infection. Kasumi-3 cells were transduced with lentiviral particles by spinfection (800xg, 1hr).
533 Since Doxycycline induction was not successful in our hands in Kasumi-3 cells, they have been
534 transduced with a non-inducible version of UL123 expression plasmid and a control mCherry
535 expression plasmid. To avoid long term effects of the transgene expression, no selection step
536 was done and the cells were treated with PMA two days after transduction followed by HCMV
537 infection two days later.

538 Quantitative real-time PCR analysis

539 For analysis of RNA expression, total RNA was extracted using Tri-Reagent (Sigma) according to
540 the manufacturer's protocol. cDNA was prepared using qScript cDNA Synthesis Kit (Quanta
541 Biosciences) according to the manufacturer's protocol. For analysis of DNA levels, cells were
542 lysed in a 1:1 mixture of PCR solutions A (100 mM KCl, 10 mM Tris–HCl pH 8.3, and 2.5 mM
543 MgCl2) and B (10 mM Tris–HCl pH 8.3, 2.5 mM MgCl2, 1% Tween 20, 1% Non-idet P-40, and 0.4
544 mg/ml Proteinase K), for 60 min at 60˚C followed by a 10 min 95˚C incubation. Real time PCR
545 was performed using the SYBR Green PCR master-mix (ABI) on the QuantStudio 12K Flex (ABI).

546 Primers spanning an exon-exon junction, were used for viral transcript quantification, for ISG
547 transcript quantification, and for the host gene Anxa5 that was used for normalization
548 (Supplementary Table 1).

549 DNA was extracted from cell pellets or directly from adherent cells in a 1:1 mixture of lysis
550 solutions A (100 mM KCl, 10 mM Tris–HCl pH 8.3, and 2.5 mM MgCl2) and B (10 mM Tris–HCl pH
551 8.3, 2.5 mM MgCl2, 0.25% Tween 20, 0.25% Non-idet P-40, and 0.4 mg/ml Proteinase K), for 60
552 min at 60˚C followed by a 10 min 95˚C incubation. Primers for the viral UL44 gene were used to
553 quantify viral DNA and a host gene (B2M) was used for normalization (Supplementary Table 1).

554 Western blot analysis

555 Cells were lysed in RIPA buffer for 30 minutes on ice and then centrifuged at 14,000 xg for 20
556 min at 4°C. Samples were separated by 4 to 12% polyacrylamide Bis-Tris gel electrophoresis
557 (Invitrogen), blotted onto nitrocellulose membranes, and immuno- blotted with the following
558 primary antibodies: mouse anti-CMV IE1 and IE2 1:1000 (abcam), mouse anti-PP28 1:2000
559 (EastCoast Bio), mouse anti-mCherry 1:1000 (ChromoTek), rabbit anti-GAPDH 1:1000 (Cell
560 Signaling Technology), rabbit anti- IRF9 1:1000 (Cell signaling Technology), rabbit anti- STAT2
561 1:1000 (Cell signaling Technology) , mouse anti- actin 1:7500 (Sigma). The secondary antibodies
562 were goat anti-rabbit–IRDye 800CW and goat anti-mouse–IRDye 680RD (LI-COR) diluted 1:7500.
563 Membranes were visualized in a LI-COR Odyssey imaging system.

564 Correlation between cellular gene expression and viral gene expression levels

565 For calculating the Spearman correlation between cellular genes and viral expression levels, in
566 each cell, the sum of viral reads was normalized to the total number of reads in the cell, and the
567 number of reads of each cellular gene was normalized to the total number of cellular reads in
568 the cell. The correlation was calculated across 313 and 310 cells on 5007 and 5606 genes for the
569 5 hpi and 12 hpi analyses, respectively. Genes with a total number of reads less than 45 (after
570 normalization to 5,000 reads per cell) were not included.

571 Differential expression and enrichment analysis

572 Differential expression analysis on bulk RNA-seq data was performed with DESeq2 (V1.22.2) [53]
573 using default parameters, with the number of reads in each of the samples as an input.
574 Differential expression analysis of the scRNA-seq was done using Seurat V4.0.3 [16]

575 The log2 fold change values were used for enrichment analysis using GSEA (version 4.1, [54]). For
576 scRNA-seq data, only genes that were expressed in at least 20% of cells in both groups of cells in
577 a comparison were used. For bulk RNA-seq, only genes that had at least 10 reads in each sample

578 were used. The gene sets that were used were Hallmark and KEGG from MSigDB (version 7.4,
579 [55]).

580 Viral gene expression heatmaps

581 Viral gene expression heatmaps depict the viral gene expression level either relative to total
582 number of viral reads (Fig. 6a) or normalized to the total number of reads (Extended Data Fig.
583 S9a). The expression levels in the heatmap are relative to the highest level of each gene.
584 Productive MDMs were ordered by their % viral reads. The cells were then grouped according to
585 the number of viral reads per bin increasing from the lowest bin to the highest bin, to ensure a
586 similar number of cells per bin. The heatmap shows the 50 viral genes with the top relative
587 expression at their highest expressing bin. Non-productive cells were grouped according to the
588 time post of infection. In each bin/time group, expression level of each viral gene was calculated
589 as the total number of reads on the gene divided by the total number of viral reads.

590 Marker staining and phagocytosis assay

591 Cells were stained in cold MACS buffer (PBS, 5% BSA, 2 mM EDTA). Cell staining was done using
592 an APC-conjugated anti-human CD11b (#101211, Biolegend), PE-conjugated anti-human CD11c
593 (#333149, BD), or FITC-conjugated anti-human CD14 (#130-080-701, Miltenyi) diluted 1:200.
594 Phagocytosis was assayed using a phagocytosis kit (#601490, Cayman chemical) according to the
595 manufacturer's instructions. The percentage of phagocytosing cells was calculated for the
596 productive and non-productive populations (as measured by GFP level) according to the flow
597 cytometry gate.

598 Graphics

599 Fig. 1f was created with BioRender. Flow cytometry figures were created with FlowJo. Fig. 3a
600 and Extended Data Fig. 4b were created with the R package ggalluvial. Figure 4d was created
601 with R package sankey.

602 Data availability

603 Sequencing data have been deposited in GEO under accession code GSE189581. Other datasets
604 analyzed in this study: Single cell RNA-seq dataset along HCMV infection of fibroblasts is
605 available under accession number GSE165291. RNA-seq dataset along differentiation of
606 monocytes to MDMs is available under accession number GSE147314. Single cell RNA-seq

607 datasets along differentiation of hematopoietic cells in the bone marrow are available under
608 accession number GSE75478 and through the Human Cell Atlas data portal at
609 https://data.humancellatlas.org/explore/projects/091cf39b-01bc-42e5-9437-f419a66c8a45.

610

611 Correspondence and requests for materials should be addressed to Michal Schwartz.

612

613 **Acknowledgements**

614 We thank Nir Drayman, Roni Winkler, and the members of the Stern-Ginossar lab, for critical
615 reading of the manuscript. We thank Dr. Keren Bahar Halpern and Dr. Shani Ben-Moshe for
616 assistance with mcSCRB-seq and 10xGenomics library preparation. We thank Eain A Murphy for
617 the TB40E-GFP virus strain. We thank the Weizmann flow cytometry unit for technical
618 assistance. This study was supported by a European Research Council consolidator grant to
619 N.S-G (CoG-2019-864012). N.S-G is a member of the European Molecular Biology
620 Organization (EMBO) Young Investigator Program.

621

622 **Author Contributions**

623 M.Sc., M.Sh., A.N. and N.S-G. conceived and designed the project, M.Sc., M.Sh., T.A., Y.K., R.L.S.
624 and M.L. performed the experiments. R.K. and R.T. provided BAL samples and advice, M.Sc.,
625 M.Sh., A.N. and N.S-G. analyzed and interpreted the data. M.Sc. and N.S-G. wrote the
626 manuscript with input from all the authors.

627

628 **Competing Interests**

629 The authors declare no competing interests.

630 **Figure 1**. Experimental system for studying HCMV infection outcome.

631 **a**. Flow cytometry analysis of primary CD14+ monocytes and monocytes differentiated with
632 PMA, infected with HCMV-GFP. Analysis was performed at 3dpi. The mock-infected GFP level is
633 marked by a line. Blue and red gates mark the GFP-dim and GFP-bright populations,
634 respectively, and their percentage is noted. **b**. ddPCR measurements of viral genomes from
635 FACS-sorted GFP-bright and GFP-dim HCMV-GFP infected MDMs at different times post
636 infection. Graph is a representative of two biological replicates and shows the mean and 95% CV
637 of poisson distribution of >10,000 PCR droplets. **c**. Measurements of infectious virus in
638 supernatants from FACS-sorted GFP-bright and GFP-dim HCMV-GFP infected MDMs, at different
639 times post infection. **d**. Flow cytometry analysis of BAL macrophages infected with HCMV-GFP at
640 3dpi. **e**. ddPCR measurements of viral genomes from FACS-sorted GFP-bright and GFP-dim
641 HCMV-GFP infected BAL macrophages at 3dpi. Graph is a representative of two biological
642 replicates and shows the mean and 95% CV of poisson distribution of >10,000 PCR droplets. **f**.
643 Experiment design. primary monocytes and PMA-induced MDMs were infected with HCMV-GFP
644 and at 5, 12, 24, 48 ,72 and 144 hpi were processed for scRNA-seq. In parallel mock-infected
645 cells from 5 and 144 hpi were also processed for scRNA-seq. **g.** Projection of HCMV-GFP infected
646 CD14+ monocytes (n=803) and MDMs (n=1815) as well as mock-infected monocytes (n=68) and
647 MDMs (n=540) from the indicated time points, based on cellular and viral gene expression,
648 colors indicate cell types and time post infection mock-infected cells are plotted in gray. **h**.
649 Projection as in **g**, showing all infected cells, colored by percentage of viral reads per cell.

650

651 **Figure 2.** Single-cell transcriptome analysis of HCMV infected macrophages.

652 **a**. Projection of 1815 HCMV-GFP infected MDMs at 5-144 hpi colored by cluster assignment.
653 Analysis was based on both cellular and viral transcripts. **b**. Projections as in figure **a**, showing
654 the cells from each time point along infection. **c**. Projection, as in **a**, colored by percentage of
655 viral reads per cell. **d**. Percentage of viral reads in single MDMs from the different clusters along
656 infection. **e**. Distribution of the single cells between the different early, non-productive and
657 productive clusters along infection. **f**. Projection of 10,320 HCMV-GFP infected myeloid BAL cells
658 from 20 and 72 hpi colored by percentage of viral reads per cell. Circles and triangles mark cells
659 from 20 or 72 hpi, respectively. Analysis was based on both cellular and viral transcripts.

660 **Figure 3.** Viral IE gene expression is a major determinant of infection outcome.

661 **a**. Cluster assignment of each cell according to analysis based on both viral and cellular genes
662 (left) or on analysis based solely on cellular genes (right). Each cell, represented by a single line,
663 is colored by the percentage of viral reads. **b**. Relative expression levels, within cells from the
664 different clusters, of viral genes from temporal classes 1 (immediate early) and 2 (true early)
665 based on [15]. **c**. Projection of infected MDMs (as in Fig. 2a) colored by the log expression level of
666 UL123 or UL122 relative to all other viral genes. **d**. Flow cytometry analysis of HCMV-GFP
667 infected THP1-derived macrophages over expressing mCherry as control, UL123, UL122 or UL99.
668 Replicate data and statistics are shown in Extended Data Fig. 4g.

669

670 **Figure 4.** Intrinsic ISG levels but not their induction affect infection outcome.

671 **a**. Projection of infected MDMs (as in Fig. 2a) colored by the expression level of ISGs. **b**.
672 Expression level of ISGs in single MDMs from the different clusters. Box plot shows standard
673 parameters (median, Q1-Q3, 1.5 IQR). p-values as calculated by one-tailed t-test on the cells in a
674 group of clusters as marked are indicated. See methods for number of cells in the analysis. **c**.
675 Viral gene expression level versus ISG expression level, in single MDMs at different times post
676 infection. The percentage of each group of cells in the given time point is indicated. **d**. Flow
677 chart describing the transition of cells between early, non-productive and productive groups
678 along infection. **e**. and **f**. Flow cytometry analysis of HCMV-GFP infected MDMs (**e**) or fibroblasts
679 (**f**) either untreated, treated with interferons at the time of infection (HCMV+IFN) or treated
680 with interferons 24 hours prior to infection (IFN-HCMV). Mock-infected cells are shown as
681 control. Replicate data and statistics are shown in Extended Data Fig. 5c, 5e, 5g and 5h. **g**. Viral
682 gene expression level versus ISG expression level in single infected monocytes, early and non-
683 productive MDMs at different times post infection. **h**. ISG expression level in mock-infected
684 monocytes and MDMs as measured from the scRNA-seq data and in mock-infected fibroblasts
685 [20]. Violin plot shows the median, Q1-Q3 (box), distribution of values (violin) and outliers. n is
686 897, 258 and 25 for fibroblasts, MDMs and monocytes, respectively. **i**. ISG expression level in
687 mock-infected cells versus viral gene expression level at early stages of infection (12 hpi or 20
688 hpi, in monocytes/MDMs and fibroblasts, respectively). p-values as calculated by one-tailed t-
689 test between cells of different types as marked are indicated. **j**. Expression levels of different

690 ISGs in cells along differentiation trajectory from monocytes to MDMs. Data taken from [23]. Violin
691 plot shows the median, Q1-Q3 (box), distribution of values (violin) and outliers. p-value as
692 calculated by one-tailed t-test comparing the cells in the first and last groups is indicated. n= 265
693 genes. **k.** Cellular transcript levels in monocytes and MDMs[23]. TPM, transcript reads per kilobase
694 per million reads mapped to cellular transcripts. **l.** Relative expression level of the viral
695 transcripts UL123 and UL22A, measured by qPCR at 12hpi, in infected MDMs either untreated
696 (HCMV) or treated with interferons 24 hours prior to infection (IFN-HCMV). Points show
697 measurement of biological replicates. p-values as calculated by one-tailed t-test on the
698 replicates are indicated. **m.** Differential expression analysis of cellular genes in uninfected THP1
699 derived macrophages (DMs) following CRISPR KO of IRF9 (left panel) or STAT2 (right panel)
700 compared to control CRISPR KO. p-values of the enrichment of ISGs in the differentially
701 expressed genes as calculated by one-tailed hypergeometric test are indicated. **n.** Flow
702 cytometry analysis of HCMV-GFP infected THP1 DMs following CRIPSR mediated knockout of a
703 control gene, IRF9 or STAT2. Two independent gRNAs were used for IRF9 and STAT2. Percentage
704 of productively infected cells are indicated for each condition. Replicate data and statistics are
705 shown in Extended Data Fig. 5n.

706

707 **Figure 5.** Effects of HCMV infection on cellular pathways and macrophage cell identity and
708 function.

709 **a**. Summary of gene set enrichment analysis (GSEA) of differentially expressed genes between
710 each of the scRNA-seq clusters and mock-infected cells from 5 hpi using annotated KEGG and
711 Hallmark pathways. Uninfected MDMs at 144 hpi are shown as control for changes occurring
712 with time in culture regardless of infection. NES- normalized enrichment score. FDR- false
713 discovery rate. **b**. Flow cytometry of CD11b surface levels in M-CSF-induced MDMs infected with
714 HCMV-GFP. The blue and red gates mark the non-productive and productive MDMs,
715 respectively, as measured by GFP level. The inset in the bottom left shows the distribution of
716 CD11b levels in the two populations. p value of the decrease in the mean fluorescence intensity
717 in GFP-bright MDMs on the measured single cells is calculated using one-tailed t-test.
718 Representative of two independent replicates is shown. **c**. Phagocytic activity measured by flow
719 cytometry of HCMV-GFP infected M-CSF-induced MDMs. The black line marks the gate for
720 identification of cells as phagocytosing. The blue and red gates mark the non-productive and

721 productive MDMs, respectively, as measured by GFP level. Replicate data and statistics are
722 shown in Extended Data Fig. 6c.

723

724 **Figure 6.** Non-productive MDMs exhibit mild elevation of gene expression with time and can
725 reactivate to produce viral progeny.

726 **a**. Heat map depicting normalized relative levels of the 50 top relatively expressed viral
727 transcripts in productive MDMs (left heatmap) and in non-productive MDMs (right heatmap).
728 Productive MDMs are binned and staged by percentage of viral reads. The expression levels in
729 the heatmap are relative to the highest level of each transcript. Viral genes are ordered based
730 on hierarchical clustering according to the productive MDMs. Annotations according to
731 temporal classes [15] are shown to the left of the heatmaps. **b**. Percentage of viral reads in single
732 non-productive MDMs along infection. Box plot shows standard parameters (median, Q1-Q3,
733 1.5 IQR). p-value as calculated by one-tailed Wilcoxon test comparing the cells in the first and
734 last groups is indicated. n is 147, 189, 165, 107 cells for 24hpi, 48hpi, 72hpi and 144hpi,
735 respectively. **c**. Number of reactivation events in HCMV infected, GFP-dim sorted, M-CSF-
736 induced MDMs following different stimulations. Points show measurements of biological
737 replicates. p-value of the increase in reactivation events upon stimuli, as calculated by one-
738 tailed t-test on the replicates, is indicated. **d**. Number of reactivation events in interferon pre-
739 treated, HCMV infected, PMA-induced MDMs either untreated or additionally stimulated with
740 PMA. Points show measurements of biological replicates. p-value of the increase in reactivation
741 events upon stimuli, as calculated by one-tailed t-test on the replicates, is indicated.

742 **References**

743 1. Staras, S. A. S. *et al.* Seroprevalence of Cytomegalovirus Infection in the United States,
744 1988-1994. *Clinical Infectious Diseases* **43**, 1143–1151 (2006).
745 2. Mocarski E, Shenk T, Griffiths P, Pass R. Cytomegaloviruses. in *Fields virology 6th ed.* (ed.
746 Knipe DM, Howley PM, Cohen JI, Griffin DE, Lamb RA, Martin MA, Racaniello VR, Roizman
747 B) 1960–2014 (Lippincott Williams & Wilkins, Philadelphia, PA., 2013).
748 3. Hahn, G., Jores, R. & Mocarski, E. S. Cytomegalovirus remains latent in a common precursor
749 of dendritic and myeloid cells. *Proceedings of the National Academy of Sciences* **95**, 3937–
750 3942 (1998).
751 4. Kondo, K., Kaneshima, H. & Mocarski, E. S. Human cytomegalovirus latent infection of
752 granulocyte-macrophage progenitors. *Proc. Natl. Acad. Sci. U. S. A.* **91**, 11879–11883
753 (1994).
754 5. Taylor-Wiedeman, J., Sissons, J. G., Borysiewicz, L. K. & Sinclair, J. H. Monocytes are a major
755 site of persistence of human cytomegalovirus in peripheral blood mononuclear cells. *J. Gen.*
756 *Virol.* **72 (Pt 9)**, 2059–2064 (1991).
757 6. Emery, V. C. Relative Importance of Cytomegalovirus Load as a Risk Factor for
758 Cytomegalovirus Disease in the Immunocompromised Host. *CMV-Related*
759 *Immunopathology* 288–301 Preprint at https://doi.org/10.1159/000061707 (1997).
760 7. Reddehase, M. J. & Lemmermann, N. A. W. Cellular reservoirs of latent cytomegaloviruses.
761 *Med. Microbiol. Immunol.* **208**, 391–403 (2019).
762 8. Ibanez, C. E., Schrier, R., Ghazal, P., Wiley, C. & Nelson, J. A. Human cytomegalovirus
763 productively infects primary differentiated macrophages. *J. Virol.* **65**, 6581–6588 (1991).
764 9. Sinzger, C., Plachter, B., Grefte, A., T. Houw The & Jahn, G. Tissue Macrophages Are
765 Infected by Human Cytomegalovirus In Vivo. *The Journal of Infectious Diseases* **173**, 240–

766 245 (1996).

767 10. Hargett, D. & Shenk, T. E. Experimental human cytomegalovirus latency in CD14+
768 monocytes. *Proc. Natl. Acad. Sci. U. S. A.* **107**, 20039–20044 (2010).

769 11. Poole, E., Reeves, M. & Sinclair, J. H. The use of primary human cells (fibroblasts,
770 monocytes, and others) to assess human cytomegalovirus function. *Methods Mol. Biol.*
771 **1119**, 81–98 (2014).

772 12. O'Connor, C. M. & Murphy, E. A. A Myeloid Progenitor Cell Line Capable of Supporting
773 Human Cytomegalovirus Latency and Reactivation, Resulting in Infectious Progeny. *Journal*
774 *of Virology* **86**, 9854–9865 (2012).

775 13. Shnayder, M. *et al.* Defining the Transcriptional Landscape during Cytomegalovirus Latency
776 with Single-Cell RNA Sequencing. *MBio* **9**, (2018).

777 14. Cheng, S. *et al.* Transcriptome-wide characterization of human cytomegalovirus in natural
778 infection and experimental latency. *Proc. Natl. Acad. Sci. U. S. A.* **114**, E10586–E10595
779 (2017).

780 15. Rozman, B. *et al.* Temporal dynamics of HCMV gene expression in lytic and latent
781 infections. *Cell Rep.* **39**, 110653 (2022).

782 16. Hao, Y. *et al.* Integrated analysis of multimodal single-cell data. *Cell* **184**, 3573–3587.e29
783 (2021).

784 17. Erhard, F. *et al.* scSLAM-seq reveals core features of transcription dynamics in single cells.
785 *Nature* **571**, 419–423 (2019).

786 18. Chaturvedi, S. *et al.* A molecular mechanism for probabilistic bet hedging and its role in
787 viral latency. *Proc. Natl. Acad. Sci. U. S. A.* **117**, 17240–17248 (2020).

788 19. Shnayder, M. *et al.* Single cell analysis reveals human cytomegalovirus drives latently
789 infected cells towards an anergic-like monocyte state. *Elife* **9**, (2020).

790 20. Hein, M. Y. & Weissman, J. S. Functional single-cell genomics of human cytomegalovirus
791 infection. *Nature Biotechnology* (2021) doi:10.1038/s41587-021-01059-3.
792 21. Reeves, M. B. Chromatin-mediated regulation of cytomegalovirus gene expression. *Virus*
793 *Res.* **157**, 134–143 (2011).
794 22. Galinato, M. *et al.* Single-Cell Transcriptome Analysis of CD34 Stem Cell-Derived Myeloid
795 Cells Infected With Human Cytomegalovirus. *Front. Microbiol.* **10**, 577 (2019).
796 23. Song, R. *et al.* IRF1 governs the differential interferon-stimulated gene responses in human
797 monocytes and macrophages by regulating chromatin accessibility. *Cell Rep.* **34**, 108891
798 (2021).
799 24. Velten, L. *et al.* Human haematopoietic stem cell lineage commitment is a continuous
800 process. *Nat. Cell Biol.* **19**, 271–281 (2017).
801 25. Setty, M. *et al.* Characterization of cell fate probabilities in single-cell data with Palantir.
802 *Nat. Biotechnol.* **37**, 451–460 (2019).
803 26. Platanitis, E. *et al.* A molecular switch from STAT2-IRF9 to ISGF3 underlies interferon-
804 induced gene transcription. *Nat. Commun.* **10**, 2921 (2019).
805 27. Munger, J. *et al.* Systems-level metabolic flux profiling identifies fatty acid synthesis as a
806 target for antiviral therapy. *Nat. Biotechnol.* **26**, 1179–1186 (2008).
807 28. Tirosh, O. *et al.* The Transcription and Translation Landscapes during Human
808 Cytomegalovirus Infection Reveal Novel Host-Pathogen Interactions. *PLoS Pathog.* **11**,
809 e1005288 (2015).
810 29. Patel, A. A., Ginhoux, F. & Yona, S. Monocytes, macrophages, dendritic cells and
811 neutrophils: an update on lifespan kinetics in health and disease. *Immunology* **163**, 250–
812 261 (2021).
813 30. Dağ, F. *et al.* Reversible silencing of cytomegalovirus genomes by type I interferon governs

814 virus latency. *PLoS Pathog.* **10**, e1003962 (2014).

815 31. Sinclair, J. Chromatin structure regulates human cytomegalovirus gene expression during
816 latency, reactivation and lytic infection. *Biochim. Biophys. Acta* **1799**, 286–295 (2010).

817 32. Yee, L.-F., Lin, P. L. & Stinski, M. F. Ectopic expression of HCMV IE72 and IE86 proteins is
818 sufficient to induce early gene expression but not production of infectious virus in
819 undifferentiated promonocytic THP-1 cells. *Virology* **363**, 174–188 (2007).

820 33. Drayman, N., Patel, P., Vistain, L. & Tay, S. HSV-1 single-cell analysis reveals the activation
821 of anti-viral and developmental programs in distinct sub-populations. *Elife* **8**, (2019).

822 34. Wu, X. *et al.* Intrinsic Immunity Shapes Viral Resistance of Stem Cells. *Cell* **172**, 423–438.e25
823 (2018).

824 35. Griffiths, P. D. Cytomegalovirus in intensive care. *Rev. Med. Virol.* **20**, 1–3 (2010).

825 36. Goodrum, F. Human Cytomegalovirus Latency: Approaching the Gordian Knot. *Annu Rev*
826 *Virol* **3**, 333–357 (2016).

827 37. Guilliams, M., Thierry, G. R., Bonnardel, J. & Bajenoff, M. Establishment and Maintenance
828 of the Macrophage Niche. *Immunity* **52**, 434–451 (2020).

829 38. Ginhoux, F. & Jung, S. Monocytes and macrophages: developmental pathways and tissue
830 homeostasis. *Nat. Rev. Immunol.* **14**, 392–404 (2014).

831 39. Poole, E. *et al.* Alveolar Macrophages Isolated Directly From Human Cytomegalovirus
832 (HCMV)-Seropositive Individuals Are Sites of HCMV Reactivation In Vivo. *J. Infect. Dis.* **211**,
833 1936–1942 (2015).

834 40. Pollock, J. L., Presti, R. M., Paetzold, S. & Virgin, H. W., 4th. Latent murine cytomegalovirus
835 infection in macrophages. *Virology* **227**, 168–179 (1997).

836 41. Baasch, S. *et al.* Cytomegalovirus subverts macrophage identity. *Cell* **184**, 3774–3793.e25
837 (2021).

838 42. Elbasani, E., Gabaev, I., Steinbrück, L., Messerle, M. & Borst, E. M. Analysis of essential viral
839 gene functions after highly efficient adenofection of cells with cloned human
840 cytomegalovirus genomes. *Viruses* **6**, 354–370 (2014).
841 43. Jackson, S. E. *et al.* Latent Cytomegalovirus (CMV) Infection Does Not Detrimentally Alter T
842 Cell Responses in the Healthy Old, But Increased Latent CMV Carriage Is Related to
843 Expanded CMV-Specific T Cells. *Frontiers in Immunology* **8**, (2017).
844 44. Keren-Shaul, H. *et al.* MARS-seq2.0: an experimental and analytical pipeline for indexed
845 sorting combined with single-cell RNA sequencing v1. *Nature Protocols* **14**, 1841–1862
846 (2019).
847 45. Jaitin, D. A. *et al.* Massively parallel single-cell RNA-seq for marker-free decomposition of
848 tissues into cell types. *Science* **343**, 776–779 (2014).
849 46. Langmead, B. & Salzberg, S. L. Fast gapped-read alignment with Bowtie 2. *Nat. Methods* **9**,
850 357–359 (2012).
851 47. Shishkin, A. A. *et al.* Simultaneous generation of many RNA-seq libraries in a single reaction.
852 *Nature Methods* vol. 12 323–325 Preprint at https://doi.org/10.1038/nmeth.3313 (2015).
853 48. Langmead, B., Trapnell, C., Pop, M. & Salzberg, S. L. Ultrafast and memory-efficient
854 alignment of short DNA sequences to the human genome. *Genome Biology* vol. 10 R25
855 Preprint at https://doi.org/10.1186/gb-2009-10-3-r25 (2009).
856 49. Bagnoli, J. W. *et al.* Sensitive and powerful single-cell RNA sequencing using mcSCRB-seq.
857 *Nat. Commun.* **9**, 2937 (2018).
858 50. Dobin, A. *et al.* STAR: ultrafast universal RNA-seq aligner. *Bioinformatics* **29**, 15–21 (2013).
859 51. van den Ent, F. & Löwe, J. RF cloning: A restriction-free method for inserting target genes
860 into plasmids. *Journal of Biochemical and Biophysical Methods* vol. 67 67–74 Preprint at
861 https://doi.org/10.1016/j.jbbm.2005.12.008 (2006).

862 52. Gibson, D. G. *et al.* Enzymatic assembly of DNA molecules up to several hundred kilobases.
863 *Nat. Methods* **6**, 343–345 (2009).
864 53. Love, M. I., Huber, W. & Anders, S. Moderated estimation of fold change and dispersion for
865 RNA-seq data with DESeq2. *Genome Biol.* **15**, 550 (2014).
866 54. Subramanian, A. *et al.* Gene set enrichment analysis: a knowledge-based approach for
867 interpreting genome-wide expression profiles. *Proc. Natl. Acad. Sci. U. S. A.* **102**, 15545–
868 15550 (2005).
869 55. Liberzon, A. *et al.* The Molecular Signatures Database (MSigDB) hallmark gene set
870 collection. *Cell Syst* **1**, 417–425 (2015).

871

figure 1

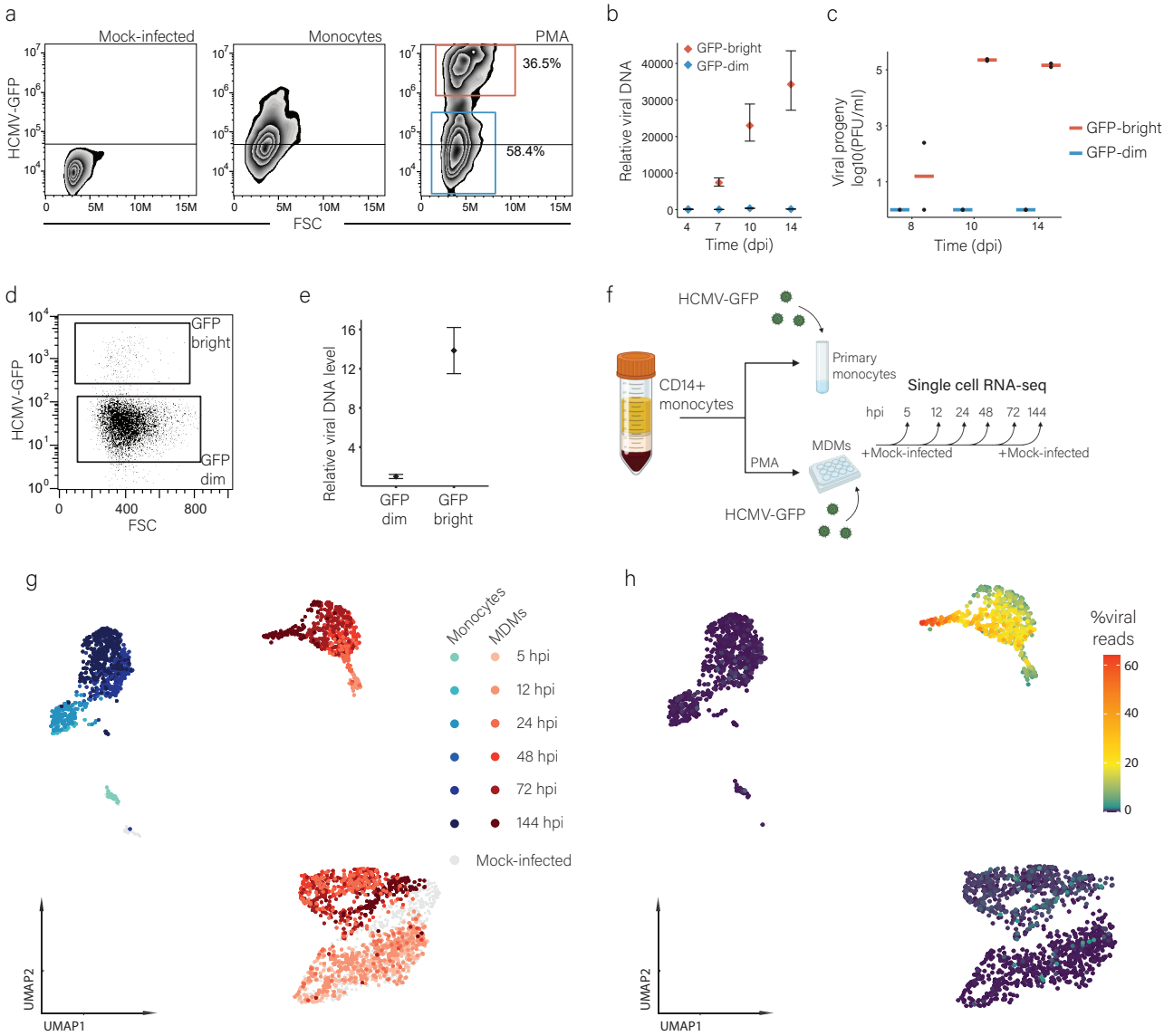
a
Mock-infected
Monocytes
PMA
HCMV-GFP
36.5%
58.4%
FSC
b
GFP-bright
GFP-dim
Relative viral DNA
Time (dpi)
c
Viral progeny log10(PFU/ml)
GFP-bright
GFP-dim
Time (dpi)
d
GFP bright
GFP dim
HCMV-GFP
FSC
e
Relative viral DNA level
GFP dim
GFP bright
f
HCMV-GFP
CD14+ monocytes
Primary monocytes
Single cell RNA-seq
hpi 5 12 24 48 72 144
MDMs
PMA
+Mock-infected
+Mock-infected
HCMV-GFP
g
Monocytes
MDMs
5 hpi
12 hpi
24 hpi
48 hpi
72 hpi
144 hpi
Mock-infected
UMAP2
UMAP1
h
%viral reads
UMAP2
UMAP1

figure 2

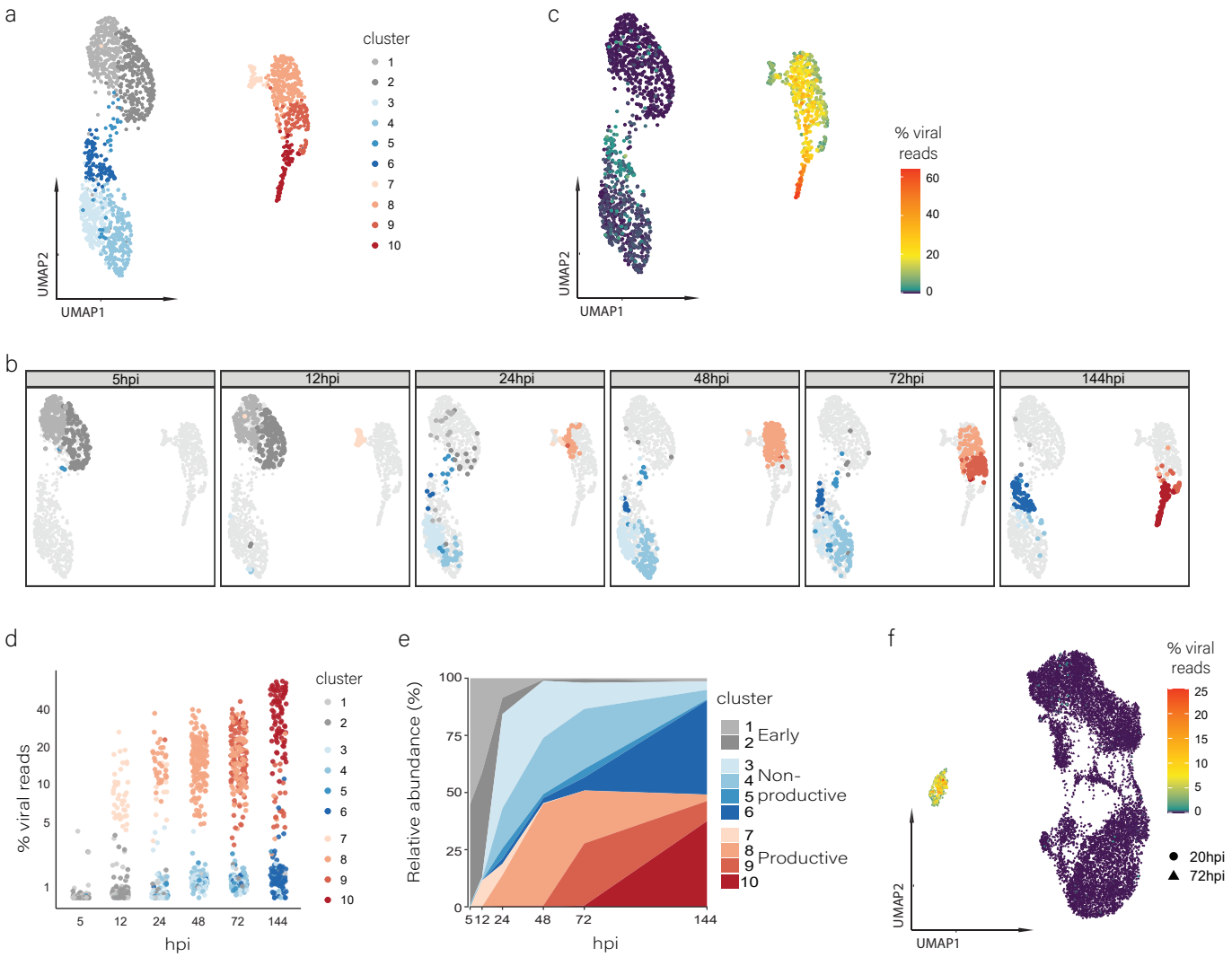
a
cluster
1
2
3
4
5
6
7
8
9
10
UMAP2
UMAP1
c
% viral reads
60
40
20
0
UMAP2
UMAP1
b
5hpi
12hpi
24hpi
48hpi
72hpi
144hpi
d
% viral reads
40
20
10
5
1
5
12
24
48
72
144
hpi
cluster
1
2
3
4
5
6
7
8
9
10
e
Relative abundance (%)
100
75
50
25
0
5
12
24
48
72
144
hpi
cluster
1
2
Early
3
4
5
6
Non-productive
7
8
9
10
Productive
f
% viral reads
25
20
15
10
5
0
20hpi
72hpi
UMAP2
UMAP1

figure 3

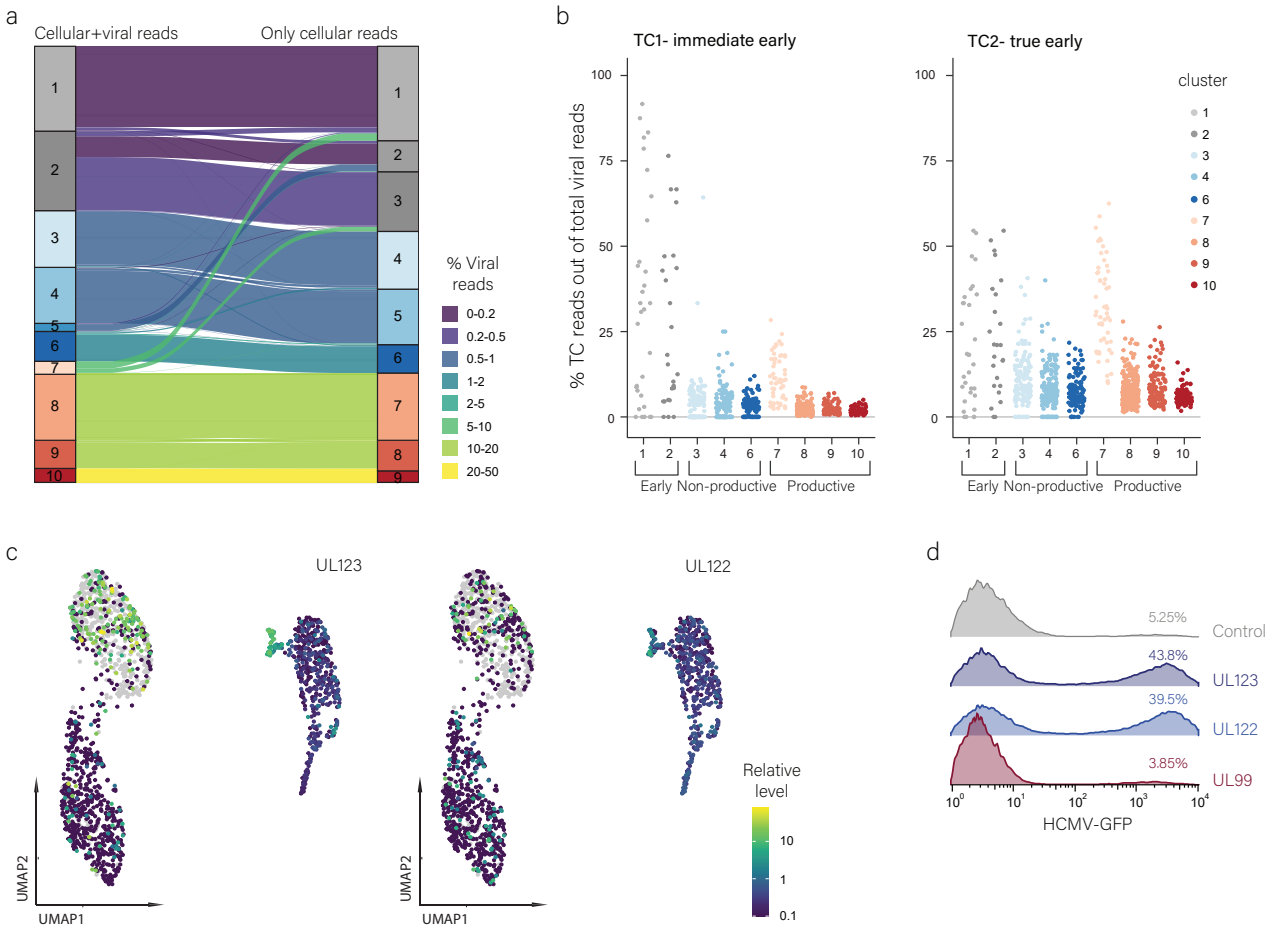
a
Cellular+viral reads
Only cellular reads
% Viral reads
0-0.2
0.2-0.5
0.5-1
1-2
2-5
5-10
10-20
20-50
b
TC1- immediate early
TC2- true early
% TC reads out of total viral reads
cluster
Early
Non-productive
Productive
c
UL123
UL122
UMAP1
UMAP2
Relative level
d
Control
UL123
UL122
UL99
5.25%
43.8%
39.5%
3.85%
HCMV-GFP

figure 4

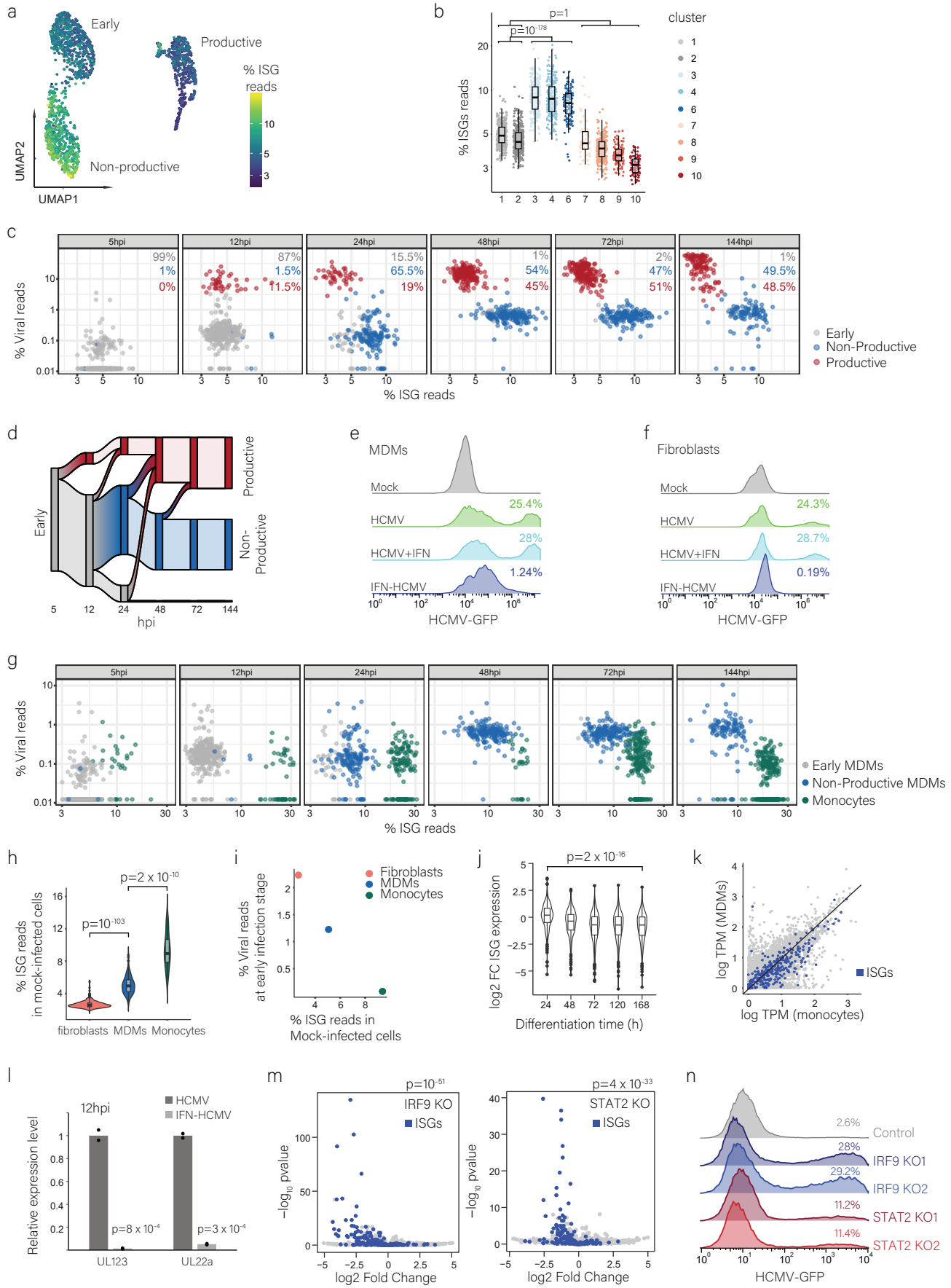
a
Early
Productive
Non-productive
% ISG reads
UMAP2
UMAP1
b
p=1
p=10^-178
cluster
% ISGs reads
c
5hpi
12hpi
24hpi
48hpi
72hpi
144hpi
% Viral reads
% ISG reads
Early
Non-Productive
Productive
d
Early
Productive
Non-Productive
hpi
e
MDMs
Mock
HCMV
HCMV+IFN
IFN-HCMV
25.4%
28%
1.24%
HCMV-GFP
f
Fibroblasts
Mock
HCMV
HCMV+IFN
IFN-HCMV
24.3%
28.7%
0.19%
HCMV-GFP
g
% Viral reads
% ISG reads
Early MDMs
Non-Productive MDMs
Monocytes
h
p=2 x 10^-10
p=10^-103
% ISG reads in mock-infected cells
fibroblasts
MDMs
Monocytes
i
Fibroblasts
MDMs
Monocytes
% Viral reads at early infection stage
% ISG reads in Mock-infected cells
j
p=2 x 10^-16
log2 FC ISG expression
Differentiation time (h)
k
log TPM (MDMs)
log TPM (monocytes)
ISGs
l
12hpi
HCMV
IFN-HCMV
Relative expression level
p=8 x 10^-4
p=3 x 10^-4
UL123
UL22a
m
p=10^-51
IRF9 KO
ISGs
p=4 x 10^-33
STAT2 KO
ISGs
−log10 pvalue
log2 Fold Change
n
2.6%
Control
28%
IRF9 KO1
29.2%
IRF9 KO2
11.2%
STAT2 KO1
11.4%
STAT2 KO2
HCMV-GFP

figure 5

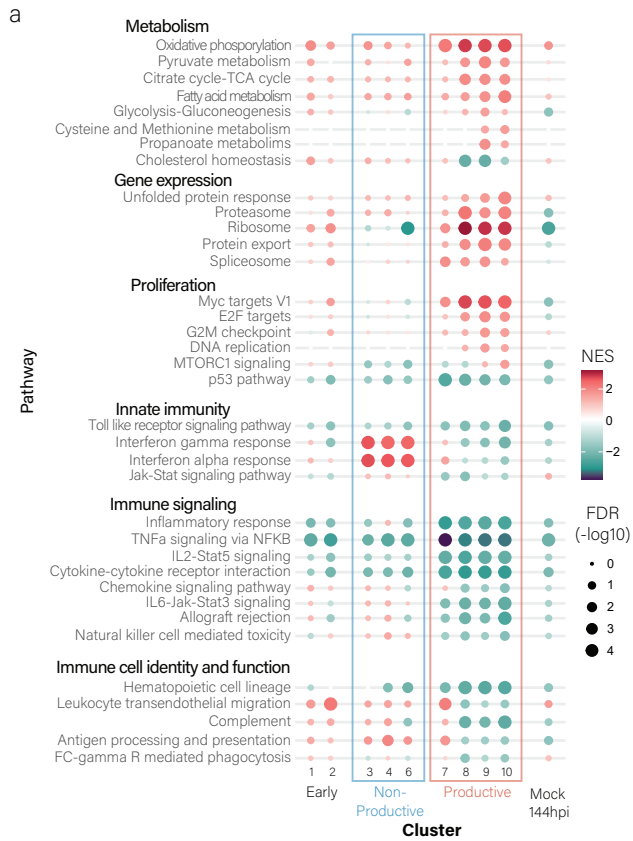
a
Metabolism
Oxidative phosporylation
Pyruvate metabolism
Citrate cycle-TCA cycle
Fatty acid metabolism
Glycolysis-Gluconeogenesis
Cysteine and Methionine metabolism
Propanoate metabolims
Cholesterol homeostasis
Gene expression
Unfolded protein response
Proteasome
Ribosome
Protein export
Spliceosome
Proliferation
Myc targets V1
E2F targets
G2M checkpoint
DNA replication
MTORC1 signaling
p53 pathway
Innate immunity
Toll like receptor signaling pathway
Interferon gamma response
Interferon alpha response
Jak-Stat signaling pathway
Immune signaling
Inflammatory response
TNFa signaling via NFKB
IL2-Stat5 signaling
Cytokine-cytokine receptor interaction
Chemokine signaling pathway
IL6-Jak-Stat3 signaling
Allograft rejection
Natural killer cell mediated toxicity
Immune cell identity and function
Hematopoietic cell lineage
Leukocyte transendothelial migration
Complement
Antigen processing and presentation
FC-gamma R mediated phagocytosis
Pathway
1 2 3 4 6 7 8 9 10
Early
Non-Productive
Productive
Mock 144hpi
Cluster
NES
2
0
−2
FDR (-log10)
0
1
2
3
4

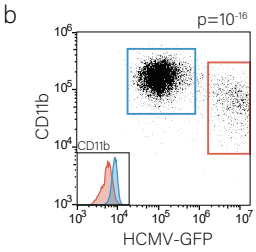
b
p=10^-16
CD11b
CD11b
HCMV-GFP

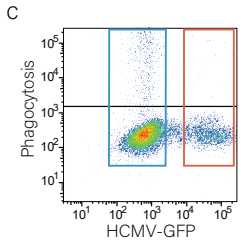
c
Phagocytosis
HCMV-GFP

figure 6

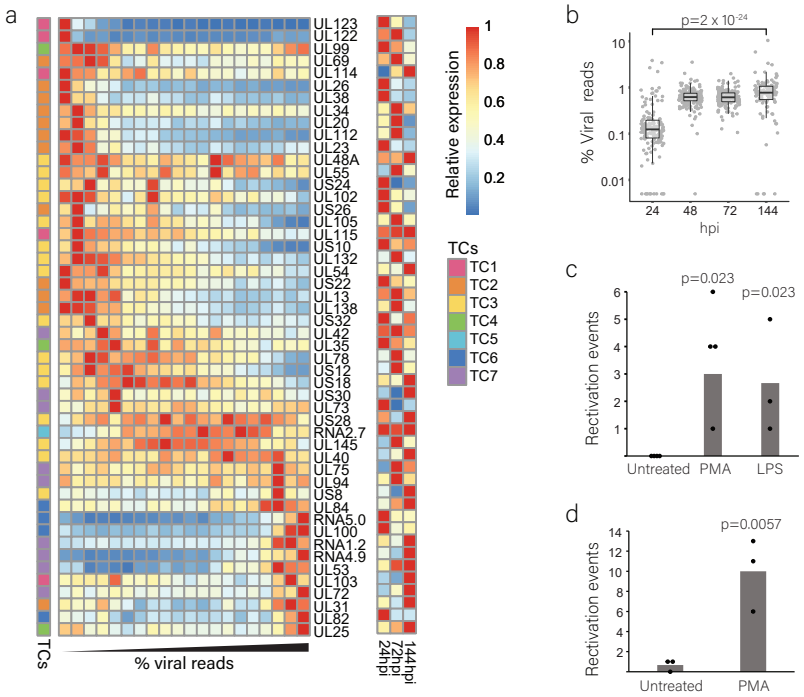
a
UL123
UL122
UL99
UL69
UL114
UL26
UL38
UL34
UL20
UL112
UL23
UL48A
UL55
US24
UL102
US26
UL105
UL115
US10
UL132
UL54
US22
UL13
UL138
US32
UL42
UL35
UL78
US12
US18
US30
UL73
US28
RNA2.7
UL145
UL40
UL75
UL94
US8
UL84
RNA5.0
UL100
RNA1.2
RNA4.9
UL53
UL103
UL72
UL31
UL82
UL25
TCs
% viral reads
144hpi
72hpi
24hpi
Relative expression
1
0.8
0.6
0.4
0.2
TCs
TC1
TC2
TC3
TC4
TC5
TC6
TC7
b
p=2 x 10-24
% Viral reads
10
1
0.1
0.01
24
48
72
144
hpi
c
p=0.023
p=0.023
Rectivation events
6
5
4
3
2
1
Untreated
PMA
LPS
d
p=0.0057
Rectivation events
14
12
10
8
6
4
2
Untreated
PMA

Extended Data figure 1

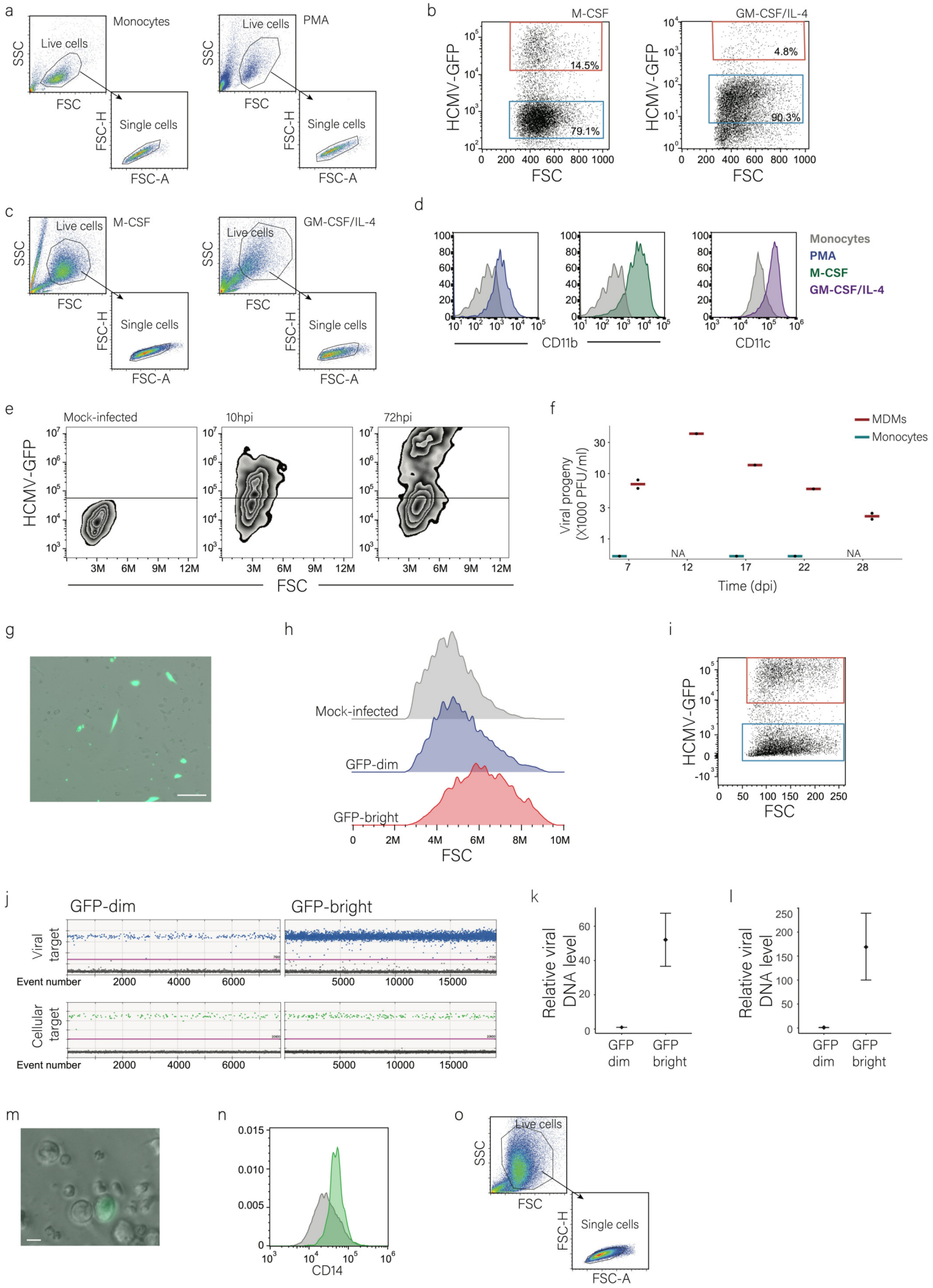

Extended Data figure 2

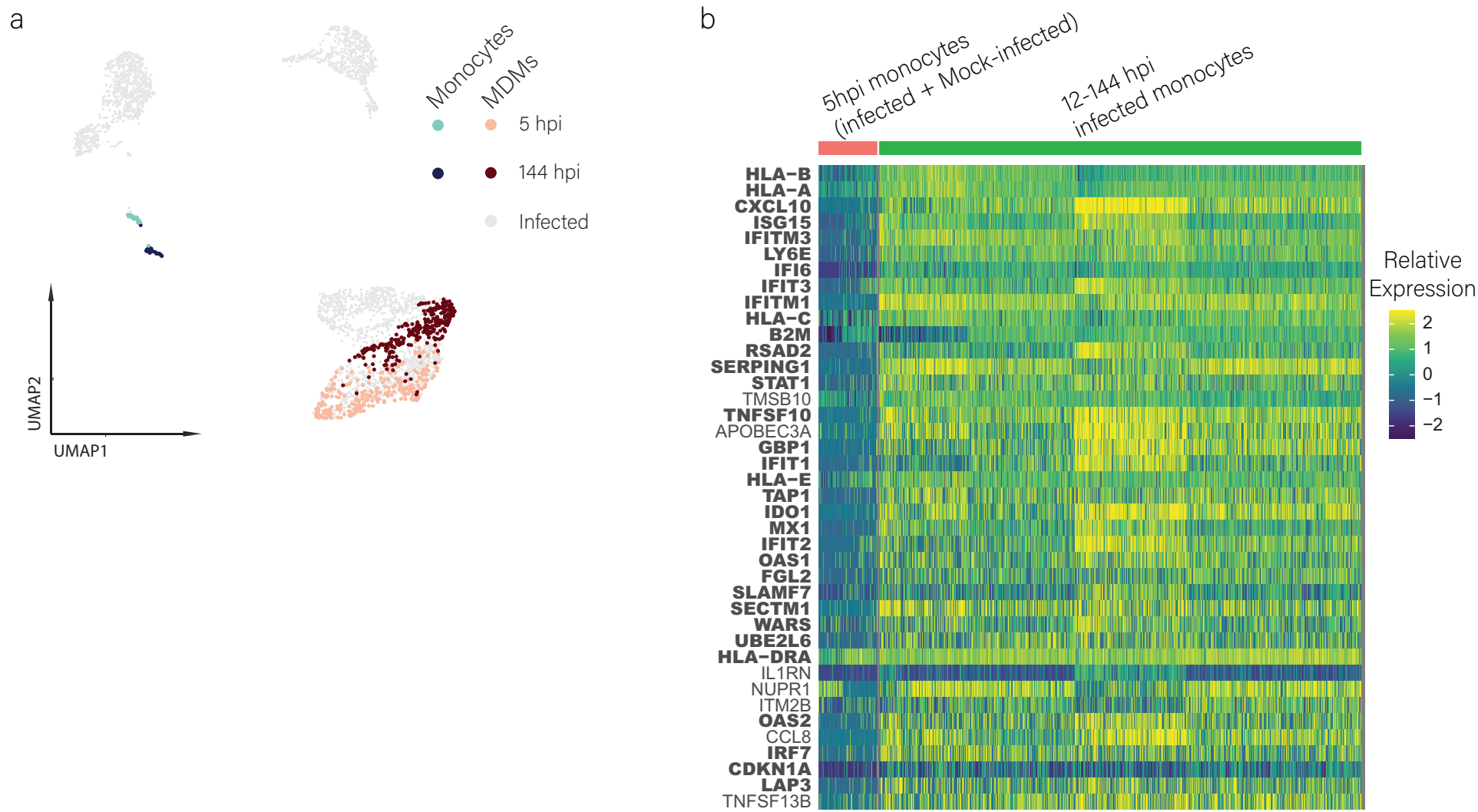

Extended Data figure 3

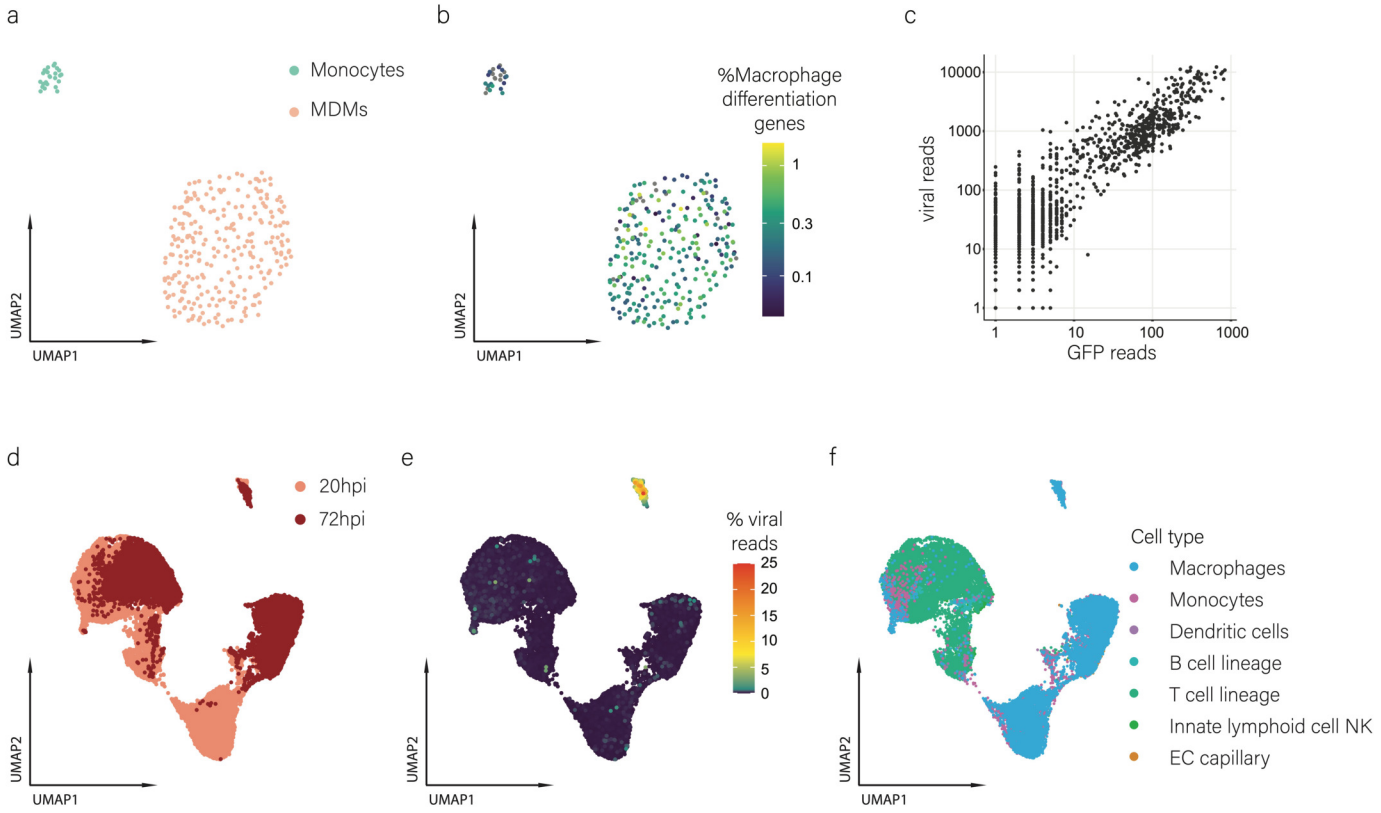

Extended Data figure 4

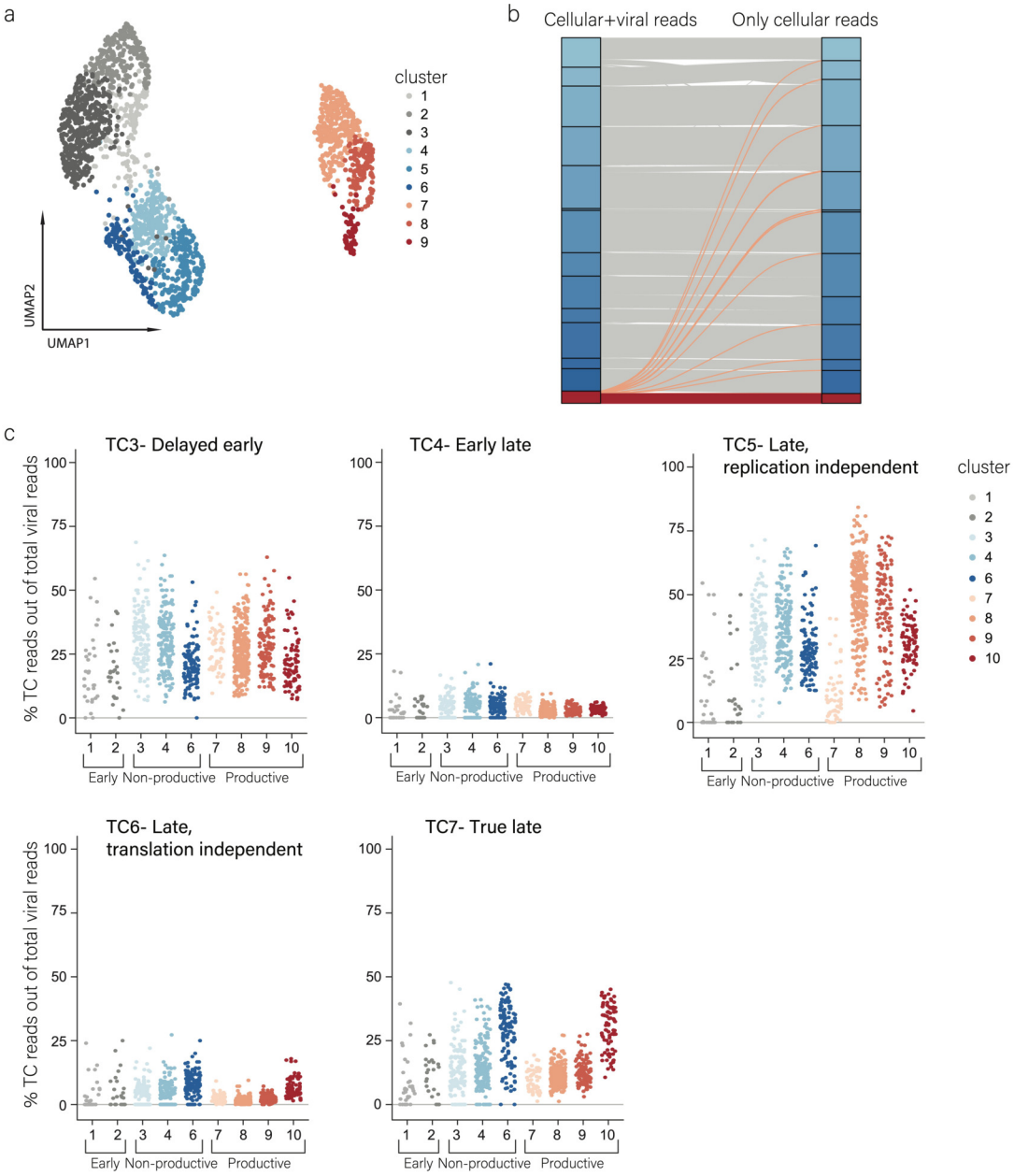

Extended Data figure 5

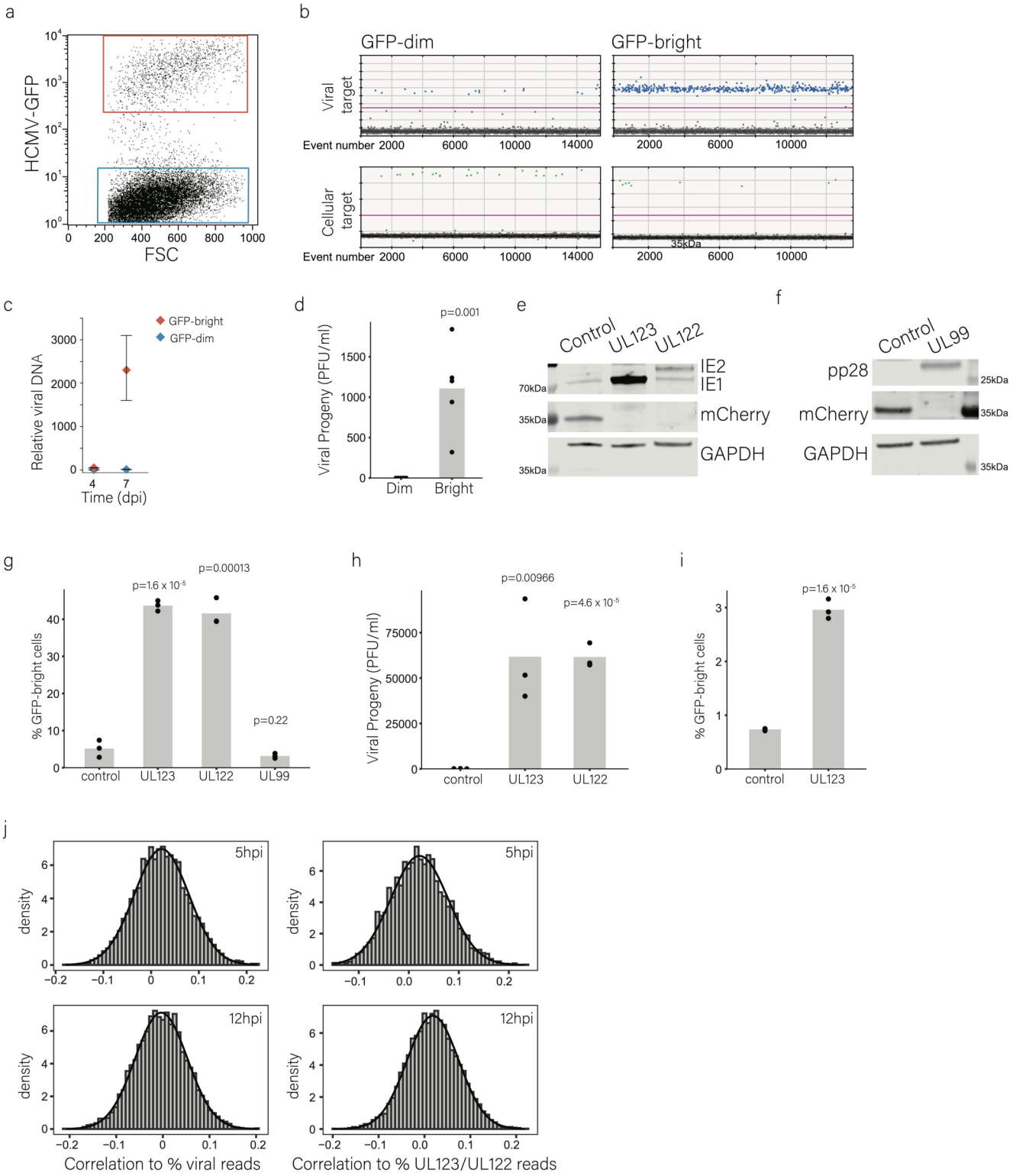

Extended Data figure 6

a

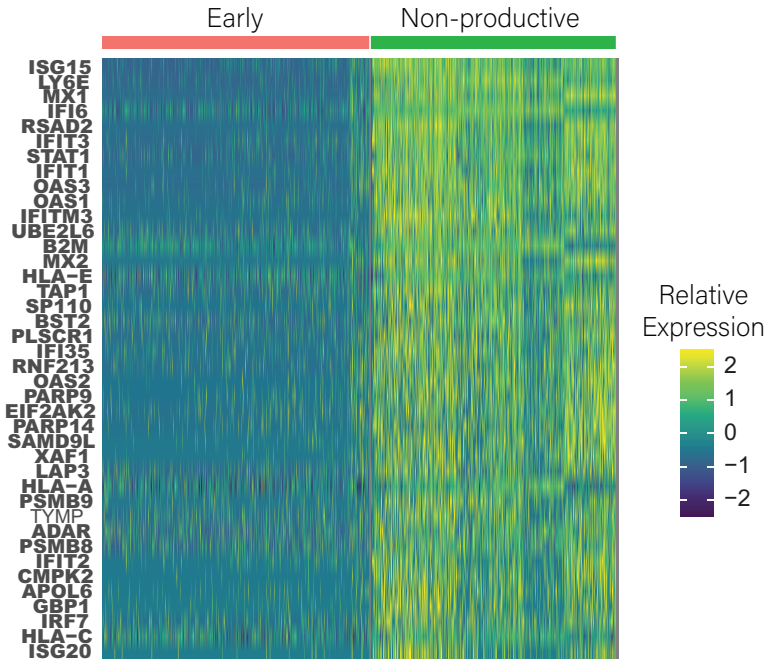

b

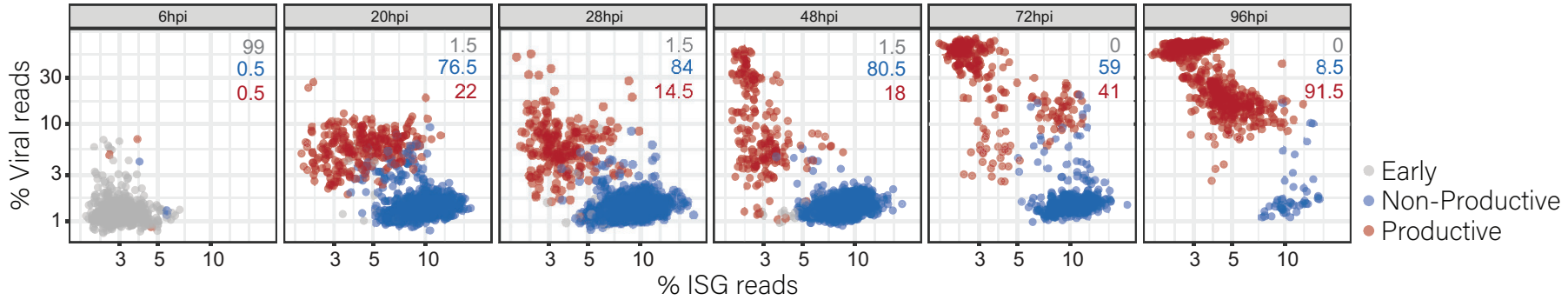

c

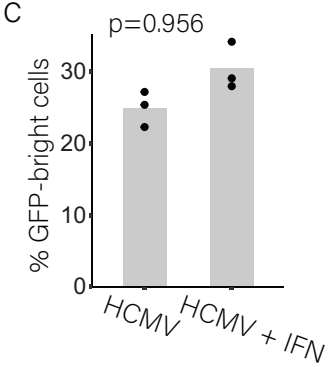

d

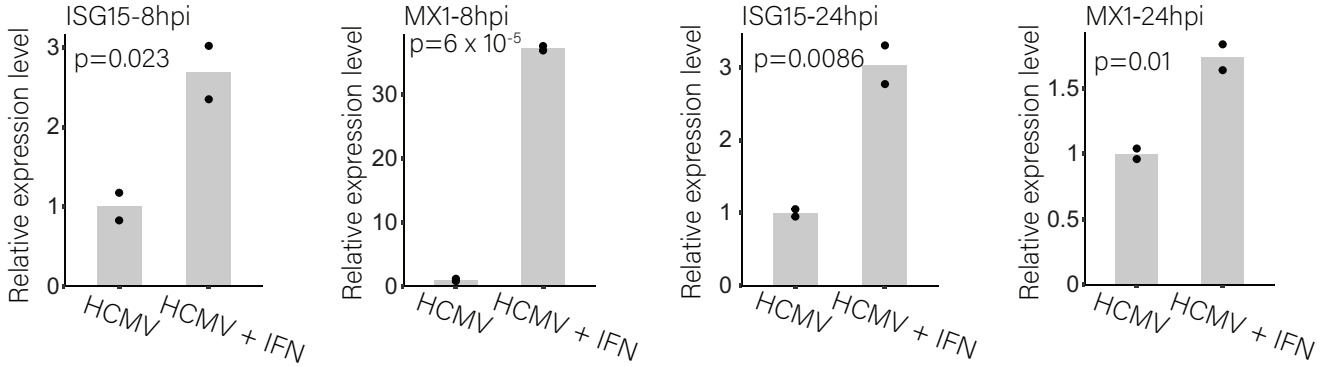

e

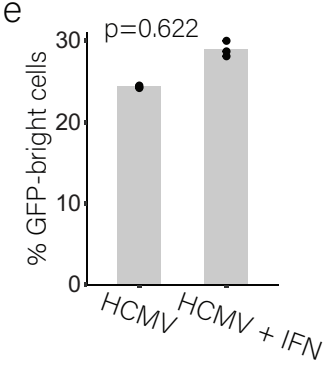

Extended Data figure 7

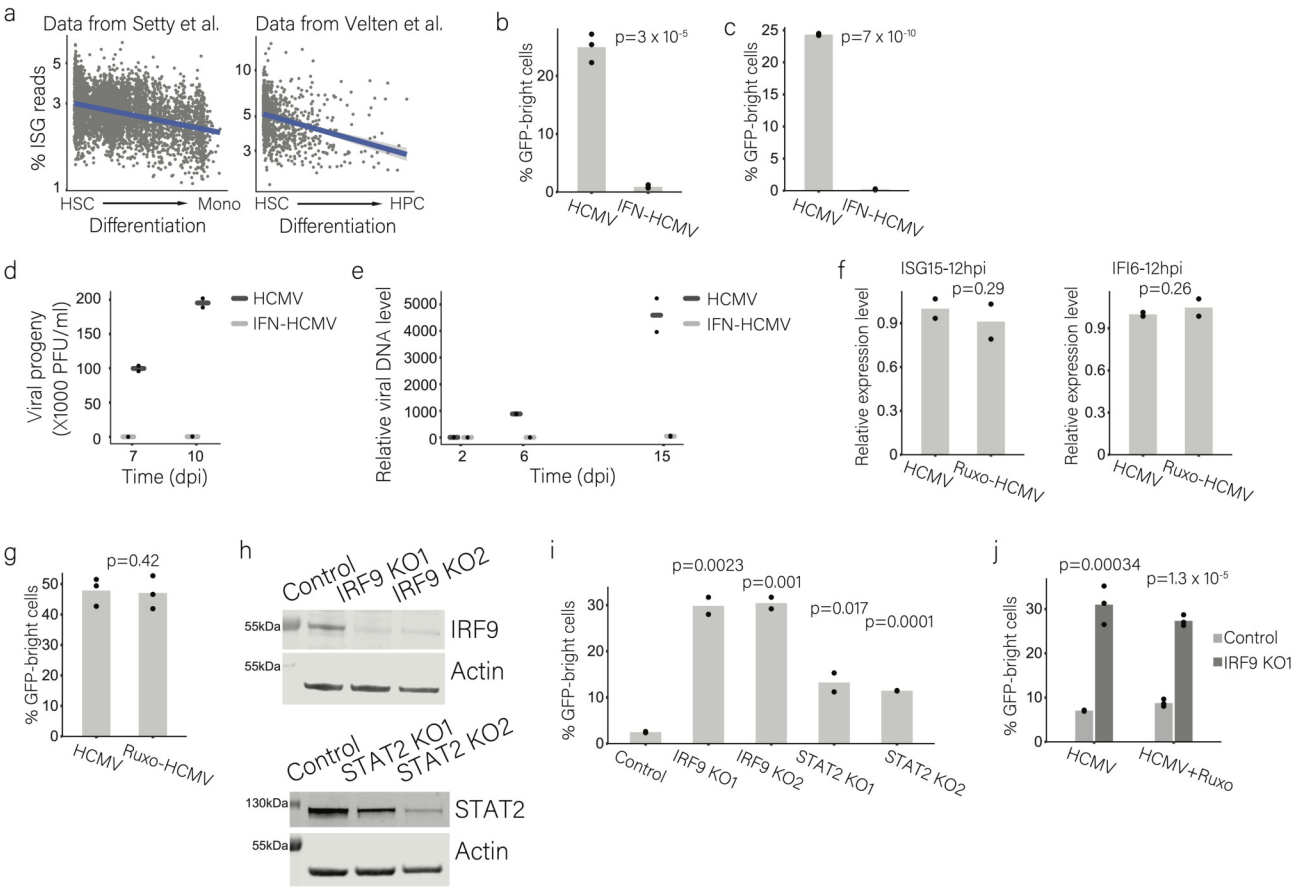

Extended Data figure 8

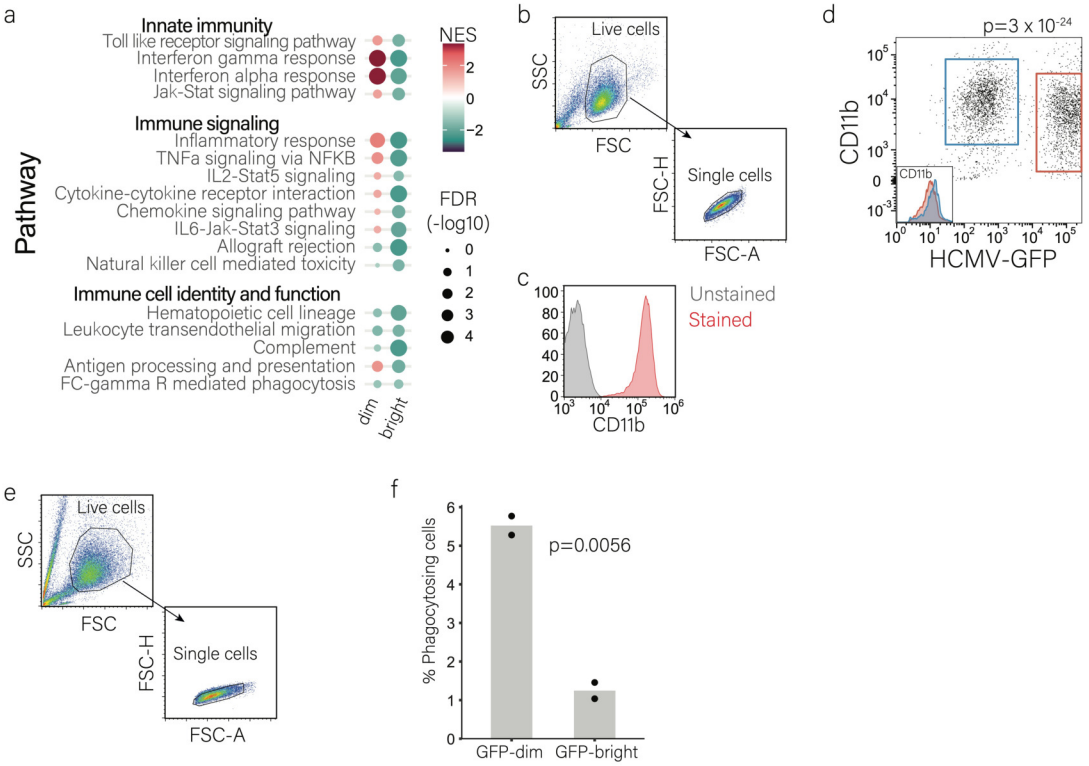
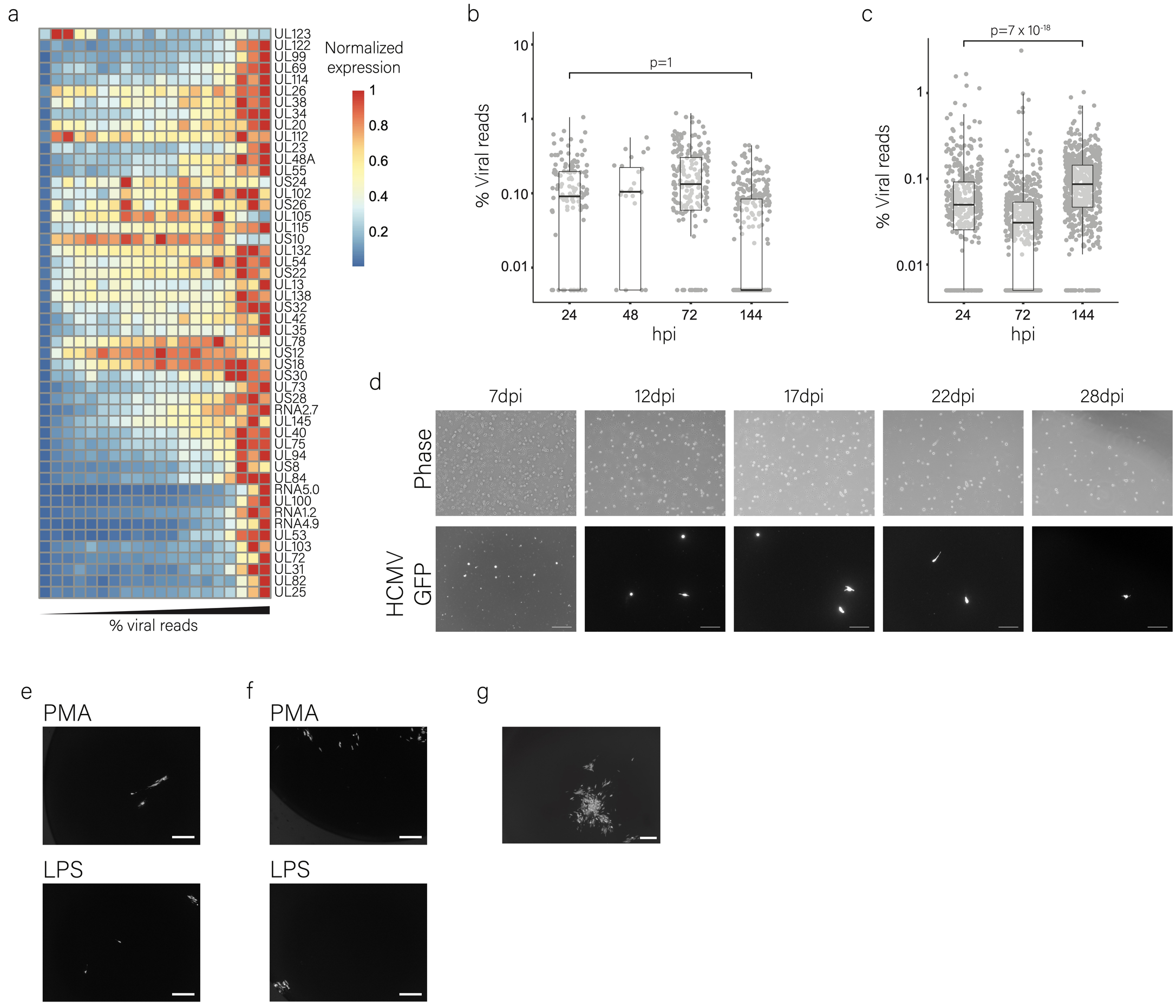
Extended Data figure 9